Naval Research Laboratory
Washington, DC 20375-5000

UNCLASSIFIED

NRL Report 9032

Preliminary Investigation of the Role That DMS and Cloud Cycles Play in the Formation of the Aerosol Size Distribution

W. A. HOPPEL, J. W. FITZGERALD, G. M. FRICK, AND R. E. LARSON

Atmospheric Physics Branch
Space Science Division

B. J. WATTLE

Advanced Technology Center
Arvin Calspan Corporation
Buffalo, New York

July 29, 1987

Approved for public release, distribution unlimited.

UNCLASSIFIED

SECURITY CLASSIFICATION OF THIS PAGE

REPORT DOCUMENTATION PAGE

1a. REPORT SECURITY CLASSIFICATION UNCLASSIFIED	1b. RESTRICTIVE MARKINGS
2a. SECURITY CLASSIFICATION AUTHORITY	3. DISTRIBUTION / AVAILABILITY OF REPORT Approved for public release; distribution unlimited.
2b. DECLASSIFICATION / DOWNGRADING SCHEDULE	
4. PERFORMING ORGANIZATION REPORT NUMBER(S) NRL Report 9032	5. MONITORING ORGANIZATION REPORT NUMBER(S)
6a. NAME OF PERFORMING ORGANIZATION Naval Research Laboratory 6b. OFFICE SYMBOL *(If applicable)* Code 4110	7a. NAME OF MONITORING ORGANIZATION
6c. ADDRESS *(City, State, and ZIP Code)* Washington, DC 20375-5000	7b. ADDRESS *(City, State, and ZIP Code)*
8a. NAME OF FUNDING / SPONSORING ORGANIZATION Office of Naval Research 8b. OFFICE SYMBOL *(If applicable)*	9. PROCUREMENT INSTRUMENT IDENTIFICATION NUMBER
8c. ADDRESS *(City, State, and ZIP Code)* Arlington, VA 22217-5000	10. SOURCE OF FUNDING NUMBERS PROGRAM ELEMENT NO. 61153N; PROJECT NO.; TASK NO. RR033-02-42; WORK UNIT ACCESSION NO. DN480-215

11. TITLE *(Include Security Classification)*
Preliminary Investigation of the Role That DMS and Cloud Cycles Play in the Formation of the Aerosol Size Distribution

12. PERSONAL AUTHOR(S)
Hoppel, W.A., Fitzgerald, J.W., Frick, G.M., Larson, R.E., and Wattle, B.J.

13a. TYPE OF REPORT	13b. TIME COVERED	14. DATE OF REPORT *(Year, Month, Day)*	15. PAGE COUNT
Interim	FROM _____ TO _____	1987 July 29	38

16. SUPPLEMENTARY NOTATION

17. COSATI CODES			18. SUBJECT TERMS *(Continue on reverse if necessary and identify by block number)*	
FIELD	GROUP	SUB-GROUP	Cloud cycles	Photooxidation
			Particle formation	Nucleation
			Vapor deposition	Photolysis

19. ABSTRACT *(Continue on reverse if necessary and identify by block number)*

A series of experiments designed to study the production of new particulate matter by photolysis of dimethyl sulfide (DMS) and the effect that nonprecipitating clouds have on the aerosol size distributions were carried out in Calspan Corporation's 600 m^3 environmental chamber during January and February 1986. The results show that DMS, the most abundant natural source of sulfur, is photooxidized to some product of low volatility that can form new particles by homogeneous nucleation or condense on existing aerosols causing them to grow.

To explain these observations, a theoretical study of the nucleation properties of methane sulfonic acid (MSA) was undertaken. The nucleation thresholds, calculated using thermodynamic data for MSA, show that at 70% RH, an MSA concentration of only 0.006 ppb will result in a supersaturated environment in which MSA will condense on preexisting particles larger than 0.02 μm radius. If the MSA concentrations increase

(Continues)

20. DISTRIBUTION / AVAILABILITY OF ABSTRACT ☒ UNCLASSIFIED/UNLIMITED ☐ SAME AS RPT. ☐ DTIC USERS	21. ABSTRACT SECURITY CLASSIFICATION UNCLASSIFIED	
22a. NAME OF RESPONSIBLE INDIVIDUAL W.A. Hoppel	22b. TELEPHONE *(Include Area Code)* (202) 767-2362	22c. OFFICE SYMBOL Code 4116

DD FORM 1473, 84 MAR 83 APR edition may be used until exhausted. All other editions are obsolete.

SECURITY CLASSIFICATION OF THIS PAGE

19. ABSTRACT (Continued)

to 30 ppb, then spontaneous formation of MSA solution droplets occurs by homogeneous binary nucleation. Simulations of the evolution of the size distribution observed for the DMS irradiation experiments with a dynamic aerosol model that includes the effects of coagulation, growth by condensation, and deposition to the walls of the chamber, yield results that are in excellent agreement with the observed evolution.

Scavenging of smaller interstitial particles by the activated cloud droplets was clearly observed in the experiment designed to simulate the effect of cloud cycles on the aerosol size distribution. Our failure to observe a clear break of the size distribution into two modes after a cloud cycling event, as previously hypothesized, probably resulted from the serious loss of cloud droplets due to fallout during the cloud cycle. In the natural environment these droplets would evaporate back down to aerosol size in the dryer air beneath the cloud. The cloud cycling experiments should be repeated with trace gases that are known to promote aqueous phase conversion of absorbed gases so that the scavenging and reevaporation of water vapor will occur on a time scale observable in the chamber before the particles fall out.

UNCLASSIFIED

CONTENTS

1. INTRODUCTION 1
   - 1.1 Background 1
   - 1.2 Chamber Experiments 1
2. INSTRUMENTATION 2
   - 2.1 Calspan's Environmental Chamber Facility 2
   - 2.2 NRL Instrumentation 3
3. DESCRIPTION OF EXPERIMENTS 4
   - 3.1 Cloud Cycling 4
     - 3.1.1 Chamber Preparation 4
     - 3.1.2 Cloud Formation 5
     - 3.1.3 Illustrative Results 5
   - 3.2 Particle Formation by Irradiation of DMS 8
   - 3.3 Addition of MSA to Chamber 13
4. THERMODYNAMICS OF MSA-WATER NUCLEATION 14
   - 4.1 Thermodynamic Data 15
   - 4.2 Heterogeneous Nucleation 18
   - 4.3 Homogeneous Nucleation 20
   - 4.4 Hydration of MSA Molecules in the Vapor Phase 20
   - 4.5 Application to Results of Irradiation Experiments 21
5. MODELING THE TIME EVOLUTION OF PARTICLE-SIZE DISTRIBUTIONS WITH A DYNAMIC AEROSOL MODEL 22
   - 5.1 Description of Model 22
     - 5.1.1 Condensation 22
     - 5.1.2 Vapor Deposition on Walls 24
   - 5.2 Description of DMS Irradiation Experiments 24
   - 5.3 Simulation of Aerosol Evolution During DMS Irradiation Experiments 25
     - 5.3.1 Inputs to Model 25
     - 5.3.2 Results of the Numerical Simulation 28
6. CONCLUSIONS 30
7. ACKNOWLEDGMENTS 31
8. REFERENCES 31

PRELIMINARY INVESTIGATION OF THE ROLE THAT DMS AND CLOUD CYCLES PLAY IN THE FORMATION OF THE AEROSOL SIZE DISTRIBUTION

1. INTRODUCTION

1.1 Background

In regions remote from continental influence, the aerosol size distribution generally has peaks at about 0.02 to 0.03 μm and at 0.08 to 0.15 μm with a minimum in the 0.05 to 0.08 μm radius range. These size distributions were first observed on a research cruise aboard the USNS *Lynch* in 1983. At that time, the peak at 0.02 to 0.03 μm radius was believed to be caused by gas-to-particle conversion and the peak at 0.08 to 0.15 μm was thought to be the result of particles generated by bursting bubbles and spray at the sea surface. Subsequent measurements of particle volatility on a cruise in 1984 aboard the NOAA ship *Discoverer* revealed that particles under both peaks were too volatile to be surface generated sea-salt particles. Four possible mechanisms which could produce a double peaked size distribution were proposed (Hoppel et al., 1985). Of the four mechanisms, the data are most consistent with the hypothesis that nonprecipitating cloud cycles play an important role in the formation of the double peaks.

Pruppacher and Klett (1978) estimate that globally the number of cloud evaporation-condensation cycles required before a precipitating system is formed is of the order of ten. Since particles in the size range under discussion are removed from the atmosphere primarily by precipitation scavenging, this would indicate, on the average, aerosol mass goes through about ten nonprecipitating cloud cycles before it is removed from the atmosphere. When an aerosol passes through a cloud cycle, the larger particles are activated and become cloud droplets. During the cloud phase, the smaller interstitial particles diffuse to and become part of the cloud droplet. Trace gases are also absorbed into and undergo chemical reactions within the droplet. When the droplet reevaporates, the residue is larger than the original particle. The net effect of the nonprecipitating cloud cycle is to produce a minimum at a size determined by the supersaturation in the cloud (Hoppel et al., 1985). Our data provide a number of evidences to support the hypothesis that nonprecipitating cloud cycles may play a major role in shaping the distribution, and that these cycles are responsible for the persistent doubly peaked feature we have observed over the remote tropical oceans. This evidence is detailed in a recent publication (Hoppel et al., 1986).

Both peaks are therefore now believed to be the result of gas-to-particle conversion. The peak at the small size results from homogeneous nucleation of new particles from gas-phase reaction products of low volatility, whereas, the peak at about 0.1 μm is primarily the result of gas phase reactions that occur in cloud droplets during the nonprecipitating cloud cycle.

1.2 Chamber Experiments

In January and February 1986, a series of experiments in Calspan's 600-m^3 environmental chamber were scheduled to test the nonprecipitating cloud cycle hypothesis by measuring the size distribution after cycling the aerosol in the chamber through repeated cloud cycles (simulated by repeated compression/expansion cycles in the humidified chamber). These experiments, which are described in this report, were not as successful as we had hoped because of the rapid fallout of cloud droplets during the cloud cycles; however, very interesting results were obtained with regard to the role that

Manuscript approved March 27, 1987.

dimethyl sulfide (DMS, CH_3SCH_3) may play in the formation and growth of marine aerosol. When DMS, a component of the natural marine environment, was introduced into the chamber and irradiated with simulated sunlight, a large number of very small particles were formed. These particles then continued to grow as long as the irradiation continued, attaining a radius of about 0.08 μm after about 6 hours. These interesting observations have led us to evaluate the chain of events that we believe occurred in the chamber experiments. Simply stated, we believe the DMS is photochemically converted to methane sulfonic acid (MSA, CH_3SO_3H) and sulfuric acid with the dominant portion being MSA. Initially the MSA and sulfuric acid concentration increases rapidly until homogeneous nucleation occurs, causing the formation of new embryos. These embryos grow by condensation of MSA and water, forming an increased surface area on which the MSA can readily condense. New particle formation ceases (when the surface area increases) and the existing particles continue to grow slowly as long as the photochemical reaction continues. Much of this report is devoted to a more quantitative description of the processes involved.

Section 3 of this report describes the results of selected experiments, with emphasis on the evolution of the size distribution during photolysis of DMS. Section 4 deals with the thermodynamic and nucleating properties of MSA, and Section 5 compares the observations with simulations using a numerical model of aerosol dynamics.

How important DMS is in the formation of particles in the remote oceanic environment has yet to be established. It does appear that if all DMS were converted to particulate mass, then DMS would be a major source of submicrometer particles. We arrive at this conclusion in the following way. The DMS flux out of the ocean surface is estimated by Andreae and Raemdonck (1983) to be about 290 $\mu g/m^2/day$. Since DMS is thought to have about a lifetime of one day, it would decompose close to its source and within the marine boundary layer. If DMS is converted uniformly to MSA (or some other condensible component such as sulfuric acid), within a 1 km boundary layer height, then the source strength of condensible material would be 0.29 $\mu g/m^3/day$. This would replenish about 3 $\mu g/m^3$ every 10 days, which is about the same timescale as the lifetime of marine aerosols (generally assumed to be between 3 and 10 days). Our data taken in the remote Atlantic indicate that the typical mass loading of particles smaller than 0.5 μm is usually in the 1 to 4 $\mu g/m^3$ range.

2. INSTRUMENTATION

2.1 Calspan's Environmental Chamber Facility

The Calspan chamber is a cylinder 9.14 m high, enclosing a volume of 590 m^3 (20,800 ft^3). The 1.25-cm-thick steel wall of the chamber is designed to withstand pressure differentials of 60 kPa (kilopascals) (6.1 m of water); however, the Pyrex cover plates of an irradiation system currently limit pressure differentials to about 3.9 kPa (40 cm of water). The inner chamber surface is coated with a fluoroepoxy type urethane developed at NRL, which has surface energy and reactivity properties comparable to those of FEP Teflon. Illumination for photochemical experiments within the chamber is provided by 28.6 kW of fluorescent blacklight and sunlamps installed inside 24 lighting modules and arranged in eight vertical channels attached to the wall of the chamber. The ultraviolet irradiation system provides an intensity based upon the photolysis of NO_2 of about K_d (NO_2) = 0.13 min^{-1}, which is about 25% of the sun's noontime intensity at midlatitudes in late summer. A complete air handling capability permits the removal of virtually all particulates (<200 Aitken nuclei/cm^{-3}) and gaseous contaminants prior to the experiment, the introduction of specified aerosols, and control of humidity from 30% to 90% RH. A rotating jet sprayer can flush the chamber with purified water with or without a detergent. Figure 1 shows the interior of the chamber. The large fan in the chamber provides circulation (if desired) to maintain uniform conditions within the chamber. The chamber has an airlock for personnel and large instrumentation as well as several observation and sample or instrument access ports. The temperature in the chamber is largely determined by the ambient temperature within the building. Note that the charcoal filters had not been reactivated for this series of experiments and therefore were not effective in removing all gaseous contaminants.

UNCLASSIFIED

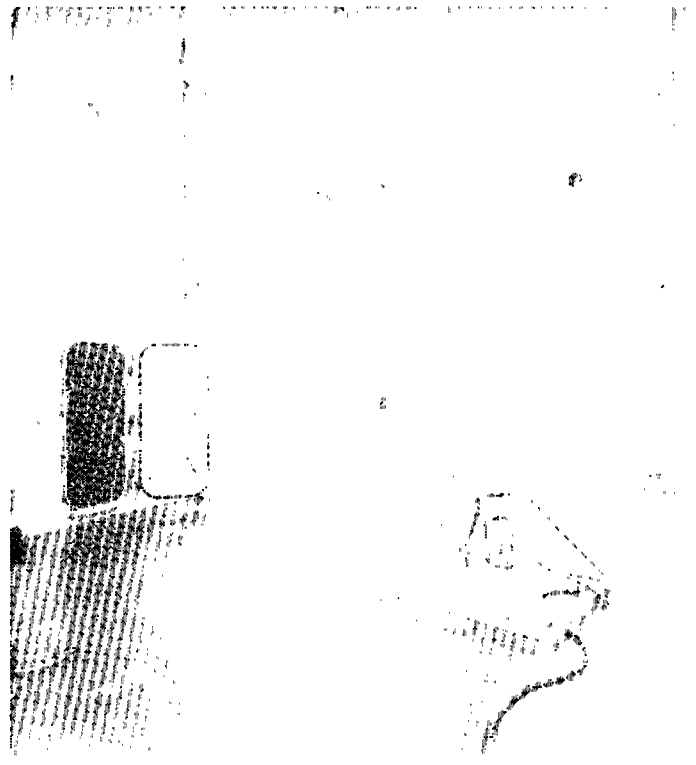

Fig. 1 — Interior of Calspan's 600 m^3 chamber

Gardner particle counters for Aitken nuclei and a Meloy Model SA260 Flame Photometric Sulfur Analyzer were set up for the experiments described in this report. Additional aerosol and gas monitoring equipment are available but were not used in these experiments. Specific details of the instrumentation and chamber facility may be found in Hanley et al., 1981 and Mack et al., 1978.

Extinction of electromagnetic radiation by aerosol hazes and fogs is measured at visible and IR wavelengths over a path of 18.3 m. For visible wavelength measurements, a lens-collimated beam from an incandescent bulb is focused on a photomultiplier detector with a peak sensitivity in the range of 0.4 to 0.5 μm wavelength. A 1.2-m path length system of similar design is also used in very dense fogs. The IR transmissometer uses a 900°C blackbody source and an HgCdTe detector operated at liquid nitrogen temperature. The source beam, chopped and collimated, is directed through the chamber (at a height of 1.2 m) and folded back to the detector by spherical front silvered mirrors. Continuous measurements of extinction as a function of wavelength are obtained to a spectral resolution of 2% over the wavelength interval from 2.5 to 14 μm; measurements are obtained at approximately 0.02 μm wavelength intervals, and data acquisition and reduction are computer controlled, with complete 2.5 to 14 μm scan requiring about 2 min.

2.2 NRL Instrumentation

The size distributions of particles between 0.006 and 0.5 μm were measured with the NRL differential mobility analyzer (Hoppel, 1978; 1981; and Hoppel et al., 1983). Particle Measurement Systems CSASP-100 and ASASP 300 probes were used to measure particle size distributions in the 0.1 to 1.5 μm (ASAS) and 0.15 to 10 μm (CSAS) radius ranges. The aerosol scattering coefficient was measured with an HSS nephelometer. Independent measurements of temperature and dew-point temperature were also made, and chamber pressure was recorded on a strip chart recorder.

3. DESCRIPTION OF EXPERIMENTS

Over 50 experiments were carried out in Calspan's chamber during 6 to 16 January and 3 to 6 February 1986. Because of the size of the chamber, much of the time for each experiment (which required a minimum of two hours) was spent in preparing the chamber and tailoring the initial size distribution to meet the objective of the experiment. The initial size distribution could be modified by a combination of procedures, such as: (a) producing particles by nebulizing salt solutions or irradiating the chamber (plus a convertible gas) with ultraviolet light, (b) flushing the chamber with outside air, or (c) filtering air through the internal filters to lower the concentration. Many of the experiments were performed to aid in the understanding of the behavior of the chamber and to establish repeatability and confidence in the measurements. For example, on two occasions the chamber was flushed with outside air (which resulted in a relative humidity of 20 to 45%) and the lights were turned on for up to 40 min. There was no observed increase in the concentration of condensation nuclei. We interpret this result as evidence that particles were not generated by heating of the lamp surfaces or by irradiation of the chamber surfaces (at least for the humidities at which these tests were performed).

Most experiments could be classified as cloud-cycling experiments, particle-formation experiments involving irradiation of DMS, or particle growth by direct addition of MSA to the chamber. One example from each of the three classes is described in detail.

3.1 Cloud Cycling

The original objective of these experiments was to test the hypothesis that nonprecipitating cloud cycles alter the aerosol size distribution to produce the double-peaked aerosol size distributions observed in the remote marine environment. The double-peaked size distribution is presumed to be due to activation of the cloud nuclei portion of the aerosol which, as cloud droplets, absorb trace gases which are converted to solid material within the droplets. If the droplets then leave the saturated environment of the cloud, their evaporation will produce particulate residues that are larger than the original nuclei.

3.1.1 Chamber Preparation

The chamber was scrubbed with detergent and rinsed with distilled water prior to this set of experiments. A fresh-air flush was usually performed in which the chamber was flushed with outside ambient air. The air was then recirculated through the filters to reduce the particle concentration to the desired level, during which warming and humidification of the air also took place.

Humidification was accomplished by spraying distilled water from a rotating nozzle mounted at the center of the chamber ceiling, which wet sheets hung on the walls and produced water puddles on the floor. The spray nozzle was operated before each set of cloud cycles for a period of approximately 30 minutes, or until a relative humidity in excess of 95% was established.

Sodium chloride solution was nebulized inside the chamber before certain experiments. A 4-ft-diameter mixing fan at the center of the chamber floor distributed the resultant aerosol throughout the chamber. The fan was turned off during the cloud cycling portion of the experiment. In addition to varying the shape of the initial size distribution, several natural gaseous contaminants (DMS, MSA, and NH_3), which we thought might convert to particulate mass within the cloud droplets, were added to the chamber.

The NRL mobility analyzer system is constructed such that its sample inlet cannot vary greatly from atmospheric pressure; therefore, it was possible to make measurements only when the chamber was at atmospheric pressure, i.e., before compression or after expansion and relaxation back to atmospheric pressure. The mobility analyzer was also fitted with a diffusion dryer at the sample inlet to measure the dry size of the particles. After several days of experiments, it was found that there

UNCLASSIFIED

was severe particle loss in the original diffusion dryer. A new dryer, which was less effective in drying the sample, but had minimal particle loss, was used in the later experiments.

The PMS probes, on the other hand, were operated continuously during the cloud cycles, with their horns oriented vertically to ensure sampling of the larger droplets.

3.1.2 Cloud Formation

Cloud formation involved pressurizing the humidified chamber, waiting for the relative humidity to rise, and expanding the humidified air. Most expansions continued until the chamber was below atmospheric pressure. Pressurization back to ambient pressure caused the cloud to dissipate rapidly.

When the clouds were formed, the PMS probes provided a visual display of the growth of activated nuclei and the large separation between the size of unactivated particles and cloud droplets that grew into the range of 3 to 15 μm radius. The mean droplet size was observed to depend upon the expansion rate and the concentration of cloud nuclei in the chamber.

Upon reevaporation of the cloud, a well-defined separation of the size distribution into double peaks as predicted by the *nonprecipitating cloud cycle hypothesis* was not observed. We view this as nondefinitive in regard to disproving the hypothesis since the cloud could only be maintained for approximately 10 minutes. A large loss of cloud droplets caused by fallout occurred in all clouds during the life of the cloud. In the natural marine environment, these droplets would evaporate back down to aerosol size in the drier air beneath the cloud.

3.1.3 Illustrative Results

The following is a detailed analysis of the results of only one of several experiments performed using a variety of initial size distributions. Figure 2 shows the scavenging of the unactivated particles by the cloud droplets and the gravitational fallout of the larger droplets. Curve 0 represents the size distribution prior to cloud formation, and curves 1 and 2 were measured after one and two cloud cycles, respectively. Note that the initial size distribution is the combined product of nebulized sodium chloride aerosol and the remnant of a previous experiment. Because of time constraints, this remnant was not completely removed by filtering and is the cause of the peak in the size distribution at 0.09 μm radius.

The chamber lamps were turned on at the start of the cloud expansion and were turned off after the expansion was completed (after 11 and 9 minutes, respectively, for the first and second clouds). It was thought that irradiation might cause chemical reactions of trace gases absorbed within the cloud droplets to form less volatile products that would remain with the particle after evaporation.

The first cloud cycle resulted in a decrease in the numbers of particles larger than 0.09 μm. This is attributed to the gravitational settling of the cloud droplets that were nucleated on these particles. A decrease in particle concentration for $r < 0.04$ μm is also evident. This decrease in the number of unactivated particles is caused by diffusion of the cloud droplets and, more importantly, to scavenging by the falling droplets, as will be discussed later. The cloud cycles had almost no effect on the concentration of particles at $r = 0.04$ μm, which would indicate that this size was below the threshold of activation for both clouds. The concentration of 0.06 μm particles diminished considerably after the first cloud cycle and very little after the second, while the peak at 0.09 μm actually increased during the second. This may be explained as follows. Particles having a radius of 0.06 μm (and larger) were activated in the first cloud cycle but not in the second. The droplets formed from the 0.06 μm particles acquired additional material by diffusion and scavenging of small particles from the gas phase, which moved them into the next larger size range ($r = 0.09$ μm) upon evaporation of the cloud, thus replenishing the particles that moved out of the 0.09 μm range during the first cloud cycle. The second cloud cycle must have produced a slightly lower supersaturation than the first (probably caused by heating of the chamber by the lamps), so that the 0.06 μm particles are now

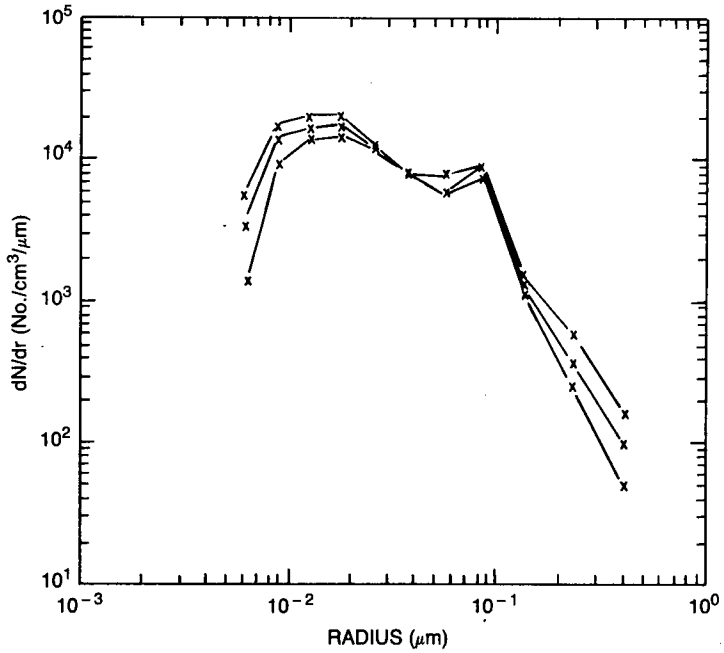

Fig. 2 — Particle size distributions measured by the differential mobility analyzer before the first cloud cycle (0), after first cloud cycle (1) and after the second cloud cycle (2)

below the threshold of activation. Now, only particles with $r \geq 0.09$ μm are activated and move into the next larger size range by acquired material, but now there are no particles moving in, thus the net reduction.

This explanation is substantiated by Figs. 3 and 4, which are particle/droplet size distributions during the first and second clouds respectively. The solid lines are soon after cloud formation, and the dotted lines are approximately 4 minutes later, which, for Fig. 4 show that the cloud has begun to evaporate. There are two lines of each type because two overlapping ranges of the instrument are plotted. The distributions contain two modes—the cloud droplets centered near $r = 5.5$ μm and some unactivated particles that have swollen to about 1-μm radius in the supersaturated environment of the cloud.

The number of cloud droplets in the first cloud is substantially greater than in the second. If both clouds were developed by the same supersaturation, then to account for the liquid water, the droplet size of the second cloud should be at least 0.5 μm larger in radius than that of the first, which does not appear to be the case.

An attempt was made to calculate the losses of interstitial aerosol during the cloud cycles. Figure 5 shows the small end of the size distribution, where the solid lines are identical to those of Fig. 2. The dotted lines represent the losses computed for diffusion to cloud droplets of radius 5 μm, where the effect of swelling on the diffusion coefficient of the unactivated particles (assumed to be sodium chloride at a relative humidity of 100%) has been taken into account by use of an equation relating the dry size to the size at 100% RH:

$$r_{100} = \left[\frac{3 B_0 r_d^3}{A} \right]^{1/2},$$

where the radii are expressed in centimeters. Here B_0 is a solubility parameter which, for NaCl, a value $B_0 = 1.3$ is appropriate. The term A incorporates the changes in vapor pressure due to surface

UNCLASSIFIED

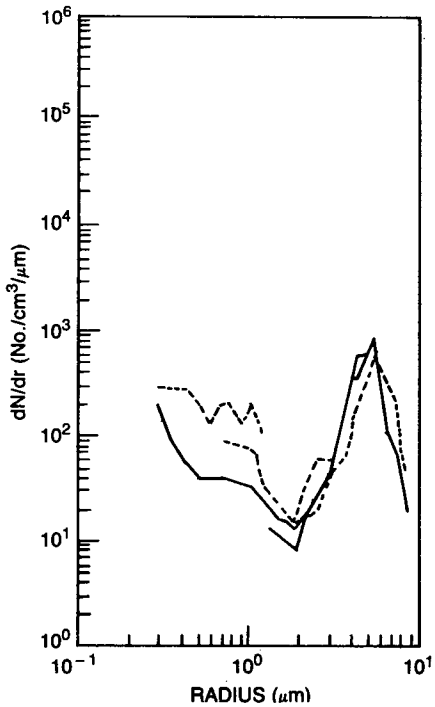

Fig. 3 — Particle size distributions measured by the particle measurement system probes during the first cloud cycle

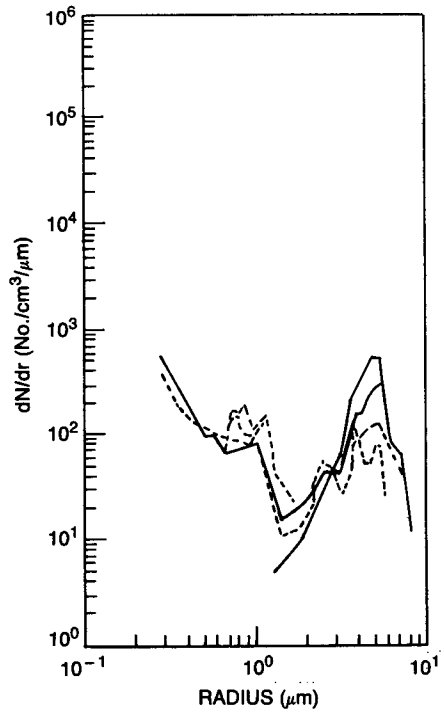

Fig. 4 — Particle size distribution measured by the particle measurement system probes during the second cloud cycle

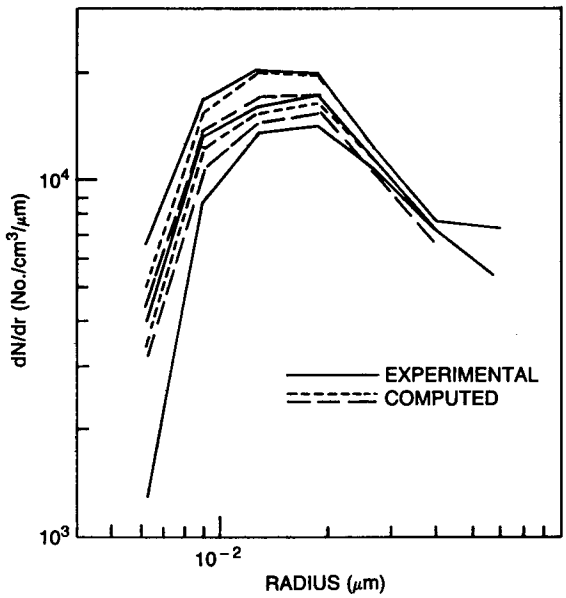

Fig. 5 — Calculated losses in interstitial aerosol during cloud cycles. Solid lines are from Fig. 2. Dotted lines are computed losses for diffusion to cloud droplets. Dashed lines represent the effect of sedimentation and/or interception.

tension, and the value $A = 1.05 \times 10^{-7}$ was determined (Fitzgerald et al., 1982). It is evident that this computation greatly underestimates the losses. Consideration of diffusiophoresis and thermohoresis to the growing/evaporating drop does not significantly alter this result. The dashed lines represent the effect of sedimentation/interception by cloud droplets which have collection and collision efficiencies of unity. The aerosol concentration as a function of radius and time was calculated from

$$n(r,t) = n_0(r) \exp\left[-4\pi a Z K(r) t\right], \tag{1}$$

where

- n_0 is the initial aerosol concentration at a given radius,
- a is the droplet radius in centimeters,
- Z is the droplet concentration,
- $K(r)$ is the collection kernel, and
- t is time in seconds.

For diffusion $K(r) = D(r)$, the particle diffusion coefficient, whereas for sedimentation $K(r) = E\pi a^2 V_{\infty,a}$ where E is the collection efficiency and $V_{\infty,a}$ is the relative velocity between particle and droplet.

Note that the loss of large particles caused by gravitational fallout of droplets during the cloud cycle and the loss of small interstitial particles not activated during the cloud cycle were consistent features of the cloud cycling experiments. However, the arguments given above regarding the behavior of the size distribution in the 0.04 to 0.1 μm range for this particular example are speculative, with very little collaborative evidence found in other cloud cycling experiments.

3.2 Particle Formation by Irradiation of DMS

During the cloud cycling experiments, DMS was added to the chamber to simulate (in exaggeration) conditions that might prevail in the marine environment. On one occasion, the irradiation lamps were turned on and within a few minutes, large concentrations of small particles were observed with the Gardner CN counter (in the absence of cloud formation). After a short time, new particle formation ceased and all existing particles continued to grow as long as the lights were on. They were observed in the smallest DMA channel (0.006 μm) after about 15 min. Because the new particle formation and growth was so dramatic, we decided to follow the evolution of the size distribution during an 8-hour irradiation period on two different occasions. The results of both 8-hour experiments were similar with regard to the evolution of the size distribution, even though there were significant differences in the initial conditions. The initial DMS concentration was 0.34 ppm for the first experiment, and an order of magnitude less at 0.04 ppm before the second experiment based on measured gaseous sulfur, whereas the initial aerosol concentration was about a factor of five greater before the second experiment.

Since the DMS irradiation experiments were not part of our original plans, we were not prepared to control other trace gas constituents in the chamber (by using the charcoal filtering capability). In fact, both experiments were carried out in the chamber after it had been flushed with outside (rural) winter air. The composition of the air in the chamber was determined by the unknown composition of the outside air plus a small remnant of air previously in the chamber.

Since the dominant features of the evolution of the size distribution were similar in both experiments, we discuss only the second experiment in detail. The differences which were observed are undoubtedly the result of different initial conditions and possible differences in trace gas composition.

UNCLASSIFIED

The DMS irradiation described here followed a series of cloud formation experiments. The chamber was flushed with outside air for 65 min. This lowered the relative humidity in the chamber, but because of the presence of water puddles on the floor, remnants from cloud experiments, the relative humidity rose to about 76% by the start of irradiation. The lamps were turned on at 1735 on 5 February, at which time the gaseous sulfur concentration was 0.04 ppm.

Particle size information is derived from differential mobility analyzer data. Size distributions were obtained automatically every 20 min throughout the period. The evolution of the size distribution is shown in Section 5 (Fig. 15) of this report where it is compared to the evolution predicted by the dynamic aerosol model. Selected particle data are plotted in Figures 6 and 7. Note Fig. 6 is a semilogarithmic plot while Fig. 7 is linear. Total particles are the sum of the particles counted in all eleven channels of the mobility analyzer. Size data are subdivided into small, medium and large particles which cover the 0.0074 to 0.022 μm, 0.022 to 0.07 μm, and 0.07 to 0.3 μm size ranges respectively. Each range consists of three DMA channels. The total particle area and volume (A and V) were computed from all particles in the size range 0.0052 to 0.3 μm.

The area and volume of the particles in the mobility analyzer size ranges are plotted in Fig. 6 and are included in Table 1.

Table 1 — Rate of Change and Relative Rate of Change of Gaseous Sulfur and Specific Volume of Particulates

Run Time (min)	Sulfur (ppm)	dS/dT (ppb/min)	dS/S (pph/h/ppm)	Vol (μcc/m^3)	dV/dT (μcc/m^3/min)	dV/dt/V (μcc/h/μcc)
0	0.0398			6.9		
30	0.0382	-0.050	-0.079	10.8	0.089	0.48
1:00	0.0367	-0.040	-0.066	13.6	0.082	0.42
1:30	0.0355	-0.040	-0.065	15.9	0.080	0.34
2:00	0.0343	-0.033	-0.058	18.1	0.078	0.26
2:30	0.0333	-0.033	-0.060	20.5	0.068	0.20
3:00	0.0323	-0.033	-0.062	22.8	0.058	0.15
3:30	0.0313	-0.027	-0.051	23.6	0.044	0.11
4:00	0.0305	-0.023	-0.046	24.4	0.030	0.07
4:30	0.0298	-0.023	-0.047	25.0	0.027	0.06
5:00	0.0291	-0.021	-0.045	25.9	0.024	0.06
5:30	0.0283	-0.022	-0.047	26.1	0.022	0.05
6:00	0.0278	-0.023	-0.050	27.0	0.021	0.05
6:30	0.0270	-0.020	-0.038	27.3	0.018	0.04
7:00	0.0264	-0.017	-0.038	27.7	0.015	0.03
7:30	0.0259					
8:00	0.0254			27.9		
8:30	0.0250	-0.007	-0.016	24.7		
9:00	0.0250	-0.005	-0.012	24.0	-0.021	-0.05
9:30	0.0248					
10:00	0.0247	-0.002	-0.004	21.7	-0.021	-0.06
11:00	0.0246			20.6	-0.019	-0.06
12:00	0.0245	-0.002	-0.004	19.5	-0.020	-0.06
13:00				18.5	-0.020	-0.06
14:00				17.5		
15:00				16.4		

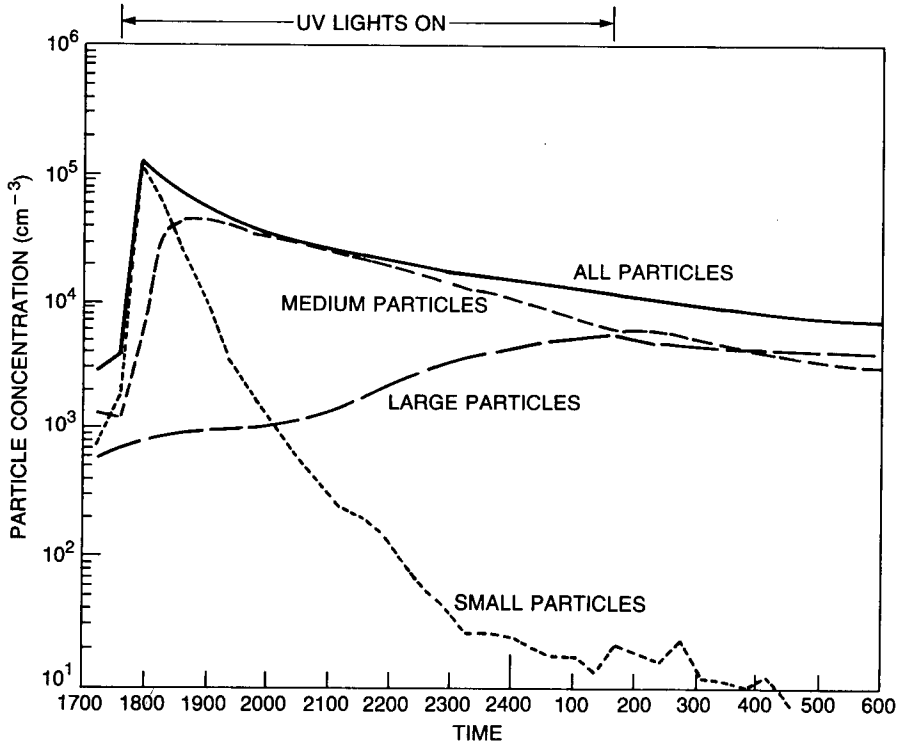

Fig. 6 — Particle size data during the DMS irradiation experiment of 5-6 February 1986. Total is the sum of particles in small (0.0074—0.022 μm), medium (0.02—0.07 μm), and large (0.07—0.3 μm) size ranges.

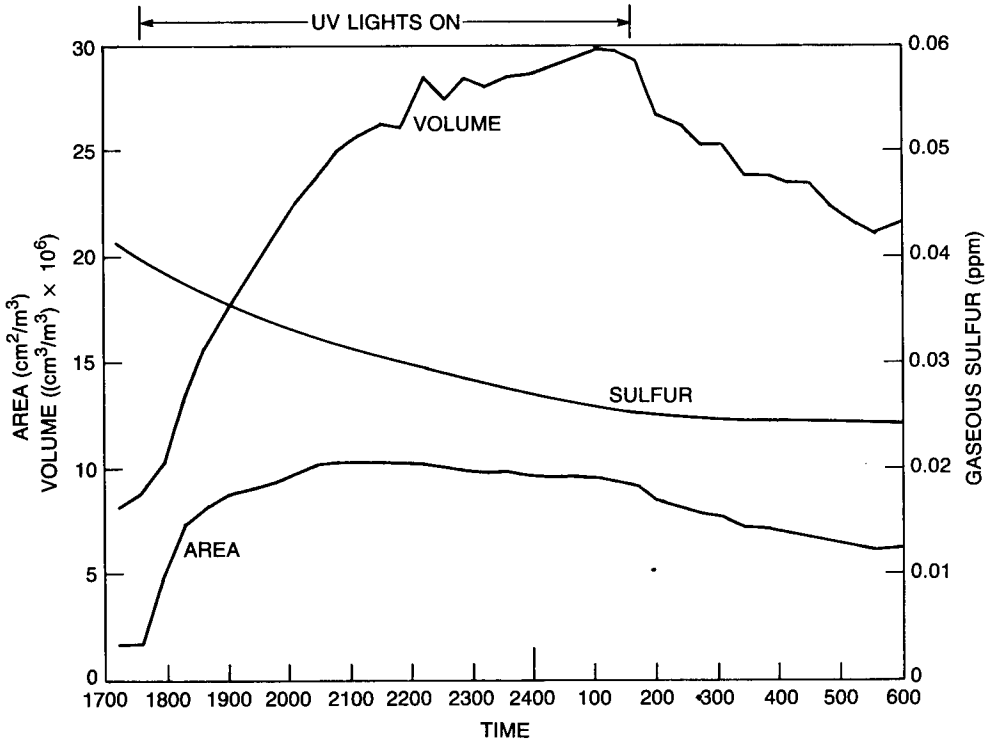

Fig. 7 — Area and volume of particles and gaseous sulfur concentration during the DMS irradiation experiment of 5-6 February 1986

UNCLASSIFIED

Particle formation was usually observed with the Gardner counter within a minute or two after the start of irradiation when DMS was present in the chamber. The first Gardner count for this experiment was 190,000/cc taken after about 6 min. About 8 min later the Gardner count was down to 100,000/cc. The maximum total particle count measured with the mobility analyzer (in the 0.006 to 0.05 μm range) occurred in the first data set completed at about 20 min. The channels are counted sequentially, thus the time between single channel readings is of the order of 20 min. Despite the poor time resolution, the data indicate that it took about 15 min for the particles to grow into the size range detectable by the mobility analyzer. After about 20 min, essentially all particles were in the mobility analyzer size range. The total DMA count increased by about a factor of 30 from 3900 (background) to 123,500 (max) particles cm^{-3}, and subsequently decreased because of coagulation of particles. The initial increase was caused by particles in the 0.0074 to 0.022-μm range (see Fig. 7). Particles in the small-size range then dropped to about 1/10 of the maximum value in about 1 hour as the particles grew through the small-size range. During this time interval, the number of medium size particles (0.022 to 0.07 μm) increased by over an order of magnitude while the total particle count decreased. The number of large particles (0.07 to 0.3 μm) increased slowly during the first 3 hours followed by a more rapid increase. After the lights were turned off, all data showed a gradual decrease with the large-particle count exhibiting the slowest decrease, which indicated that the primary loss mechanism is probably diffusional loss to the walls and not gravitational settling.

We believe these experiments are evidence that the photooxidation of DMS results in a product that has an extremely low volatility. Initially the concentration of this new material is so large that homogeneous nucleation of new particles occurs. After sufficient particle surface area is generated, the condensation of the material on existing particles lowers its concentration below the homogeneous nucleation threshold. Existing particles continue to grow as long as the photooxidation continues to produce condensable material.

Recently, Hatakeyama et al. (1985) found evidence that the photooxidation of DMS resulted in about 20% of the DMS sulfur being converted to SO_2 with the rest converting to MSA. As shown in the next section of this report, MSA-water solution condensate forms at 90% RH when the MSA concentration reaches only 0.0001 ppb (10^{-13} atm). In addition, the presence of SO_2, most likely will lead to the formation of H_2SO_4, which is even less volatile than MSA and could be the agent (together with MSA and possibly traces of NH_3) that causes the homogeneous nucleation of new particles.

The total gaseous sulfur decreased from 0.04 to 0.025 ppm (or about 40%) during the 8 hours of irradiation. The rate of decrease slowed from 0.05 ppb/min at the start to 0.02 ppb/min at the end of the irradiation, then slowed to 0.002 ppb/min with no irradiation. Thus the conversion of DMS was apparently concentration-dependent during the irradiation. (This was not the case during the first experiment when there was a much higher DMS concentration.) The fractional rate of decrease of gaseous sulfur after the lights were turned off for over 1 hour was 0.004 ppb/h/ppb. Note that although the sulfur concentration was almost an order of magnitude larger for the first experiment, the fractional loss after irradiation (0.003 ppb/h/ppb) was the same within the accuracy of the data on both days. Since DMS is a volatile gas that is nearly insoluble in water, we would expect very low deposition velocities once the chamber reaches equilibrium. If we assume that the loss is to the chamber walls, then we can compute a deposition velocity of 3×10^{-4} cm/s for DMS in the chamber.

Note also that although the initial sulfur concentration was down by about a factor of ten at the start of this experiment as compared to the first DMS irradiation experiment, the initial rate of decrease in sulfur was only down by a factor of two. This is probably because the direct photolysis of reduced sulfur compounds such as DMS is unlikely, and the reaction mechanism involves some other rate limiting step such as the production of excited oxygen atoms or hydroxyl radicals (Cox and Sandalls, 1974). In the presence of nitrogen oxides, OH may be efficiently regenerated by photolysis (Sze and Ko, 1980). Hatakeyama et al. (1985) had 1.3 ppm DMS and 0.7 ppm NOx as initial concentrations, and the DMS was depleted within 4 hours using an irradiation source only three times as intense.

The total integrated particle volume increased at a rate of about 0.08×10^{-6} cm^3 m^{-3} min^{-1} at the start and about 0.02 toward the end of irradiation. After irradiation ceased, particle volume decreased, the decrease stabilized at about 0.02×10^{-6} cm^3 m^{-3} min^{-1}. The fractional rate of decrease of particle volume after irradiation ceased was 6% h^{-1}. This fractional decrease of particle volume (like the fractional rate of decrease of total gaseous sulfur) was the same as the first experiment within measurements uncertainties and implies wall losses.

The depletion of gaseous sulfur can be equated to the increase in particulate mass if loss to chamber walls is neglected. MSA is thought to be a product of the atmospheric oxidation of DMS (Saltzman et al., 1983). Hatakeyama et al. (1985) found evidence of both MSA and sulfuric acid in the aerosol generated by the irradiation of DMS. For the following approximate calculations, the exact proportion of MSA to sulfuric acid (about 4:1) are unimportant.

A steady-state mass balance 2 h into the irradiation can be estimated by comparing the net sulfur loss of 0.03 ppb/min (0.033 increase less 0.002 after irradiation) with particle production. At 20°C, 1 ppb of a gas is about 2.5×10^{16} molecules/m^3. Thus the sulfur loss and assumed MSA (molecular weight 96.11) production was about 7.5×10^{14} molecules/min/m^3 or 12×10^{-8} g/m^3/min ($7.55 \times 10^{14} \times 96/(6 \times 10^{23})$). Since MSA takes up about double its weight of water at the relative humidity of the experiment, then equating sulfur loss to MSA droplet production predicts a mass increase of 36×10^{-8} g/m^3/min, assuming no losses to the chamber surfaces. The concurrent net rate of volume increase of particles measured by the mobility analyzer was 8×10^{-8} cc/m^3/min. Allowing for the 2×10^{-8} losses after lights off, the gross production was 1×10^{-8} cc/m^3/min. Assuming a density of 1.2 g/m^3 corresponding to droplets of 6% mole fraction solutions of MSA, the mass increase of the volume distribution is 12×10^{-8} g/m^3/min. The resultant ratio of particle volume increase to that predicted by DMS loss is about one third, which we consider to be relatively good agreement considering the accuracy of this calculation. Section 5 of this report shows that the difference in loss of DMS and the increase in particle mass can be accounted for by wall loss if the MSA vapor is assumed to have a deposition velocity of 12 cm/s.

Pich et al. (1970) show that with a constant rate of gas-to-particle conversion the surface area reaches a constant value such that the rate of formation of surface area by condensation is equal to the rate of loss by coagulation. If the size distributions are self-preserving, then there are simple relationships between the surface area A, volume V, and number N of aerosol particles. For coagulating aerosols smaller than the molecular mean-free-path without simultaneous gas-to-particle conversion, the relation $A/((N^{1/3})\ (V^{2/3}))$ should be 4.35 for a self-preserving distribution. It is also expected (McMurry and Friedlander, 1986) that there will not be much variation even when condensation is occurring, especially in the later stages of aerosol formation.

The ratio $A/((N^{1/3})\ (V^{2/3}))$ calculated from our size distributions increased slowly throughout the irradiation period. The ratio approached to within 5% of the self-preserving value after 3 h of irradiation, but did not reach 4.35 until close to the end of the irradiation. The self-preserving ratio of 4.35 was maintained throughout the approximate 8 h of size distributions after the irradiation stopped. Similar results were obtained from data for the first DMS irradiation experiment. Note that the rate of volume increase was constant for the first 4 h of irradiation and then slowed noticeably. The area began to show a slow decrease after the volume increase slowed noticeably. The deviation in volume from the expected constant rate of volume increase, and in the area reaching and maintaining a maximum, can be attributed to the reaction being dependent upon the concentration of sulfur. During the first experiment (when the DMS concentration was greater), the volume had increased at a constant rate throughout the entire irradiation and the area was approaching an asymptotic value late in the irradiation period.

If the rate at which DMS is photooxidized is assumed to be first order, then a value for the first-order-rate constant k for the photodecomposition of DMS can be computed from a linear fit to the plot of sulfur concentration as a function of time on semilog paper. A value of 0.07 h^{-1} was calculated for k (and hence a mean lifetime for DMS of 14 h) under irradiation intensity equal to about

UNCLASSIFIED

25% of the sun's noontime intensity by assuming that 20% of the DMS was converted to SO_2 and that the lifetime of SO_2 in the gaseous state is long compared to that of DMS. The relevance of this value for the first-order-rate constant to the real atmosphere is unknown because of the uncertain compositions of trace gases that may have been in the chamber and may have influenced the reaction mechanism.

3.3 Addition of MSA to Chamber

Methane sulfonic acid was added directly to the chamber on several occasions by placing 1 to 3 ml in an evaporation dish held at an elevated temperature by contact of the dish with a water reservoir. The evaporation dish was located close to the mixing fan. There was no experimental determination of the amount of MSA that evaporated. The original solution was 80% MSA and appeared to be more viscous than the solution removed, indicating the uptake of water by the MSA during the experiment. On every occasion when the MSA was evaporated at temperatures between 80° and 100°C, there was a moderate initial increase in the number of particles. More dramatic was the continuous growth of existing particles as long as the MSA was in the chamber. Removing the MSA stopped the growth immediately, replacing the MSA (at the elevated temperature) initiated the growth. We believe the moderate increase in particles is caused by binary homogeneous nucleation of MSA and water vapor which occurs because of the high MSA concentration which must exist very near the evaporation dish. Particle growth is caused by condensation of MSA and water vapor on the existing particles by the mechanism discussed in Section 5 of this report.

The first experiment on 3 February 1986 illustrates the effect of direct evaporation of MSA into the chamber. The chamber was flushed with fresh air for 55 min, and the initial conditions before adding MSA to the air were: 43% RH and an aerosol count of 1100 per cm^3. At 1010, 1 ml of MSA in an evaporation dish in contact with water at 99°C was placed in the chamber and allowed to remain there for 20 min. The Aitken nuclei count increased to 2100 cm^3 after 2 min, 3200 cm^3 after 5 min, reached a maximum of 6500 cm^3 after 15 min, and was at 5100 when the MSA was removed from the chamber after 20 min. Figure 8 shows the particle size distributions measured immediately before and after the MSA was in the chamber and illustrates the rapid growth of particles in the presence of a small quantity of MSA.

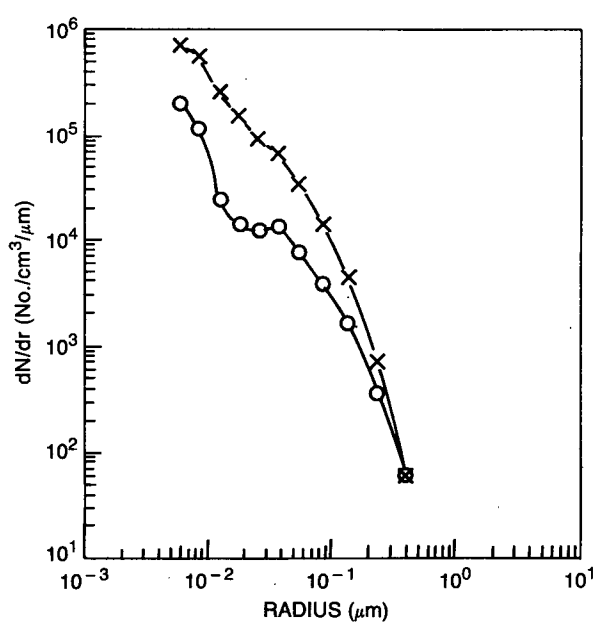

Fig. 8 — Particle size distributions before (0) and after (x) addition of MSA to the chamber

Figure 8 is consistent with the interpretation that new particles were formed at small sizes and that all particles were growing by binary condensation of MSA and water vapor. Diffusional growth theory predicts that radial growth is inversely proportional to the radius, so that very little growth is observed for particles with large radii.

The mass of the particles as computed from the size distribution increased from 9.6 to 18.4 $\mu g/m^3$. If this observed increase in aerosol mass is to be attributed to MSA, then the loss of MSA by evaporation must be at least as great as the observed increase in aerosol mass. The evaporation rate can be estimated in the following way. The vapor pressure (in atmospheres) of MSA as a function of temperature is estimated from the following equation:

$$\ln P_{\mathrm{MSA}} = 15.8 - \frac{8870}{T} , \tag{2}$$

where T is the temperature in Kelvins and the constants were determined by using the data of Clegg and Brimblecombe (1985) at 25°C and from the CRC handbook at 122° and 167°C. The total mass flux is then given by:

$$F = P_{\mathrm{MSA}} A \, \mathrm{v}_e , \tag{3}$$

where $P_{\mathrm{MS}A}$ is the saturation vapor density obtained from Eq. (2), A is the surface area of MSA in the dish, and v_e is the evaporation velocity (opposite of deposition velocity).

The surface area of the MSA was about 2 cm^2, and the deposition velocity as estimated in Section 5 of this report is 12 cm/s. This gives a mass flux of 20 $\mu g/s$. Dividing the mass flux by the volume of the chamber gives a volume source rate of 2 $\mu g \ m^3 \ min^{-1}$ of MSA. From the deposition velocity, area of the chamber, number and size of the particles, one can estimate that about three to four times as much MSA condenses on the walls as condenses on the particles. Thus the source rate available for particle growth is about 0.5 $\mu g \ m^{-3} \ min^{-1}$. From the results of Section 4 of this report, the MSA concentration of the aerosol for the relative humidity of the chamber is about 0.15 mole fraction. Accounting for the mass of the water, the volume source rate is about 1 $\mu g \ m^{-3} \ min^{-1}$. In 20 min this would add 20 $\mu g \ m^{-3}$ as compared to 9 $\mu g \ m^{-3}$ increase observed in the size distribution. This calculation is meant only as an order-of-magnitude estimate, but it does show that it is not unreasonable to assume the aerosol growth is the result of direct condensation of MSA solution onto the particles.

4. THERMODYNAMICS OF MSA-WATER NUCLEATION

Naturally produced DMS is the most abundant source of organic sulfur in the atmosphere. The global yearly injection of DMS from the oceans is estimated to be about 40×10^{12} g, which is about one-half the estimated anthropogenic emission of SO_2 (Andreae and Raemdonck, 1983). Since most of the SO_2 is emitted over the continental regions of the northern hemisphere, the importance of DMS as a source of sulfur in the remote oceanic regions and in the southern hemisphere must be relatively large and could account for most of the non-sea-salt sulfate in marine aerosols. Hatakeyama et al. (1985) conducted experiments that indicated that the photooxidation of DMS gives about 21% SO_2 with the remaining sulfur being converted to MSA. Experiments by the same authors show that the photooxidation of DMS in humid air (35% RH) containing 12 ppb DMS and 6 ppb NO produced large concentrations of particles in which both MSA and sulfuric acid were detected in the particles.

It is well known that certain gas-phase reactions produce reaction products that have low volatility. When these new species reach some critical concentration, the atmosphere becomes supersaturated with respect to that species and condensation occurs on existing particles. If the concentration continues to increase, homogeneous nucleation of new embryos occurs at some critical concentration. If the nucleation process involves more than a single molecular species, as is usually the case in

UNCLASSIFIED

the atmosphere, then the nucleation is heteromolecular and the resultant particle is a solution or compound of unique proportions determined by the environmental vapor pressures of the condensing species. The simplest type of heteromolecular nucleation is binary nucleation of solution droplets. Of particular importance in the atmosphere is the water-sulfuric acid system, which has been explored by a number of authors (for example, see Reiss, 1950; Mirabel and Katz, 1974; Heist and Reiss, 1974; Hoppel, 1975).

The growing awareness of the potential importance of DMS/MSA in the formation of atmospheric aerosols and the need to interpret experiments involving the formation of MSA aerosol makes this a propitious time to investigate the thermodynamics of nucleation in the MSA-water system.

The free energy of formation of a solution embryo of radius r containing n_1 moles of component one and n_2 moles of component two is (see Mirabel and Katz, 1974).

$$\Delta G = n_1(\mu_{1L} - \mu_{1g}) + n_2(\mu_{2L} - \mu_{2g}) + 4\pi r^2 r \,, \tag{4}$$

where σ is the surface tension, μ_{1L} and μ_{1g} (μ_{2L} and μ_{2g}) are the chemical potentials of component one (two) in the liquid and gaseous state respectively. This expression can be rewritten in terms of mole fraction of solute x and the fugacities f (Hoppel, 1975)

$$\Delta G = 4\pi r^2 \sigma(x) - \left[\frac{1-x}{M_1(1-x)+M_2 x}\right] \frac{4}{3}\pi r^3 \rho_L(x) RT \ln \left[\frac{f_{1g}}{f_{1L}(x)} \left(\frac{f_{2g}}{f_{2L}(x)}\right)^{\frac{x}{1-x}}\right] , \tag{5}$$

where M_1 and M_2 are the molecular weights, $\rho_L(x)$ is the density of the droplet and depends on the mole fraction x, R is the gas constant, and T is the temperature. At pressures of interest in the atmosphere, the fugacities can be equated to the vapor pressures so that f_{1g} and f_{2g} are the vapor pressures in the atmosphere and $f_{1L}(x)$ and $f_{2L}(x)$ are the equilibrium vapor pressures of the solution.

We have chosen to express ΔG in terms of the variables x and r, rather than in terms of n_1 and n_2 because it is conceptually more convenient to think in terms of critical radius and concentration when dealing with heterogeneous nucleation of preexisting nuclei, which are usually characterized by their radius. The (n_1,n_2) coordinate system has the advantage that the Gibbs-Duhem relationship can be used to simplify the mathematical expressions for an analytical treatment. For numerical computations, we have found it more convenient to use (r,x) coordinates.

4.1 Thermodynamic Data

To evaluate the free energy of formation of a MSA-water embryo from the vapor, the environmental vapor pressures of MSA and water must be known together with the following thermodynamic data.

• *The equilibrium vapor pressure of both water* $[f_{2L}(x)]$ *and MSA* $[f_{gL}(x)]$ *as a function of MSA concentration.* The osmotic coefficient and MSA activity coefficient have been measured by Covington et al. (1973). The water vapor pressure of the solution can be obtained directly from the osmotic coefficient ϕ from

$$f_{1L} = P_o \exp\left(-\frac{2m\phi}{55.5}\right) , \tag{6}$$

where P_o is the vapor pressure of pure water and m is the molal concentration. However, the vapor pressure of the MSA cannot be obtained directly from the activity coefficient without a measurement of the MSA vapor pressure of the reference state. Recently Clegg and Brimblecombe (1985) have

measured the vapor pressure of concentrated solutions of MSA and estimated the equilibrium constant to be 6.5×10^{13} mole^2 kg^{-1} atm^{-1}. The equilibrium vapor pressure of MSA is therefore obtained from

$$f_{2L}(m) = \frac{m^2\gamma^2}{6.5 \times 10^{13}}, \tag{7}$$

where γ is the activity coefficient. Values of the osmotic coefficient and activity coefficient (from Covington et al.) and the derived equilibrium vapor pressures are given in Table 2.

Table 2 — Thermodynamic Properties of MSA

Molality	Mole Fraction	Osmotic Coef.	Sat. Ratio	Activity Coef.	Vapor Pressure (atmos.)	Density (g/cm^3)	Surface Tension (dyne/cm^2)
0.10	0.0018	0.950	0.9966	0.807	1.00×10^{-16}	1.00145	71.8
0.20	0.0036	0.955	0.9931	0.785	3.79×10^{-16}	1.00532	71.3
0.30	0.0054	0.965	0.9896	0.779	8.40×10^{-16}	1.00913	70.8
0.40	0.0071	0.975	0.9861	0.779	1.49×10^{-15}	1.01291	70.4
0.50	0.0089	0.984	0.9824	0.783	2.36×10^{-15}	1.01664	69.6
0.70	0.0124	1.005	0.9750	0.799	4.81×10^{-15}	1.02396	69.1
1.00	0.0177	1.039	0.9633	0.833	1.07×10^{-14}	1.03464	67.9
1.50	0.0263	1.091	0.9428	0.901	2.81×10^{-14}	1.05161	66.3
2.00	0.0348	1.139	0.9213	0.980	5.91×10^{-14}	1.06762	64.8
2.50	0.0431	1.195	0.8980	1.071	1.10×10^{-13}	1.08273	63.6
3.00	0.0512	1.248	0.8739	1.179	1.92×10^{-13}	1.09699	62.6
3.50	0.0593	1.311	0.8477	1.307	3.22×10^{-13}	1.11045	61.7
4.00	0.0672	1.356	0.8226	1.430	5.03×10^{-13}	1.12317	60.9
5.00	0.0826	1.459	0.7690	1.736	1.16×10^{-12}	1.14657	59.6
6.00	0.0975	1.556	0.7145	2.097	2.44×10^{-12}	1.16753	58.5
7.00	0.119	1.641	0.6613	2.504	4.73×10^{-12}	1.18636	57.7
8.00	0.1259	1.714	0.6104	2.948	8.56×10^{-12}	1.20334	57.1
9.00	0.1394	1.776	0.5624	3.423	1.46×10^{-11}	1.21871	56.5
10.00	0.1526	1.827	0.5180	3.920	2.36×10^{-11}	1.23268	56.1
12.00	0.1776	1.931	0.4342	5.105	5.77×10^{-11}	1.25713	55.4
14.00	0.2013	2.001	0.3647	6.353	1.22×10^{-10}	1.27788	54.9
16.00	0.2236	2.067	0.3040	7.796	2.39×10^{-10}	1.29578	54.5
18.00	0.2447	2.114	0.2541	9.288	4.30×10^{-10}	1.31144	54.2
20.00	0.2647	2.155	0.2119	10.910	7.32×10^{-10}	1.32526	54.0
25.00	0.3104	2.176	0.1411	14.480	2.02×10^{-9}	1.35330	53.6
30.00	0.3507	2.148	0.0983	17.470	4.23×10^{-9}	1.37369	53.4
35.00	0.3865	2.106	0.0704	19.900	7.46×10^{-9}	1.38821	53.2
40.00	0.4186	2.058	0.0516	21.940	1.18×10^{-8}	1.39941	53.1

For our calculations of the free energy, the activity coefficient and osmotic coefficient data of Covington et al. were fitted to polynomials and Figs. 9 and 10 show the results.

• *The density as a function of MSA concentration.* Teng and Lenzi (1975) have published density data and fitted their data to a polynomial. However, their polynomial fit did not extend to concentrations high enough for our homogeneous nucleation calculations. A sixth-order polynomial covering the range from 0 to 0.4 mole fraction was fit to data taken from the supplemental data tables of Teng and Lenzi. Values of density calculated from this polynomial fit are given in Table 2.

UNCLASSIFIED

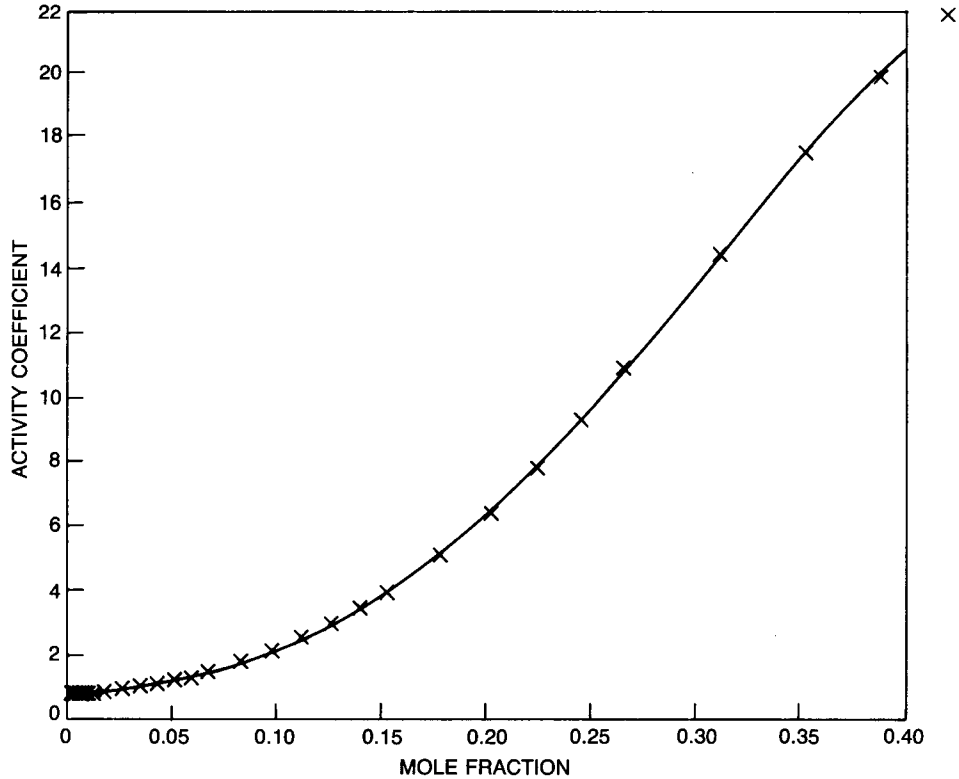

Fig. 9 — Fourth-order polynomial fit to the activity coefficient data (x) of Covington et al. (1973)

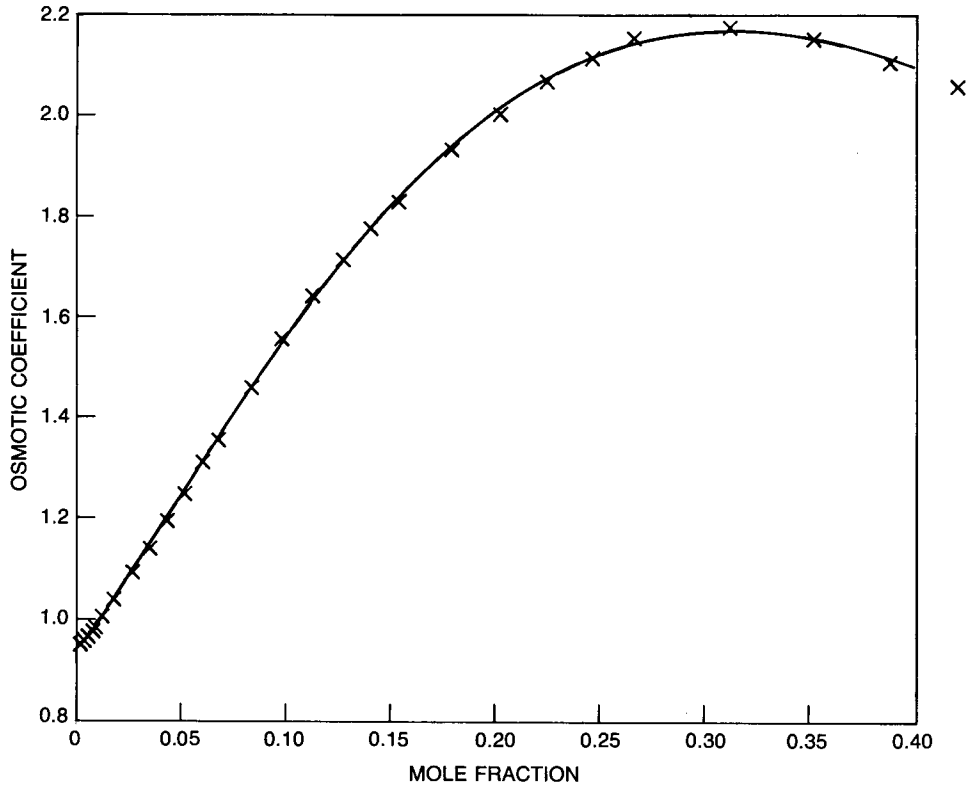

Fig. 10 — Fifth-order polynomial fit to the osmotic coefficient data (x) of Covington et al. (1973)

• *Surface tension as a function of MSA concentration.* We were unable to find any published values of surface tension for MSA solutions. For the case of pure MSA at about 37° and 73°C values of surface tension are given by Berthoud (1929). Figure 11 shows the data points from the recent measurements made at NRL. A polynomial fit to the data in powers of $\ln(x+1)$ was used in our calculations of free energy from Eq. (5).

$$\sigma = 51.777 - 3.7628 \ln(x+0.1) + 4.51915[\ln(x+0.1)]^2 - 2.93893[\ln(x+0.1)]^3. \quad (8)$$

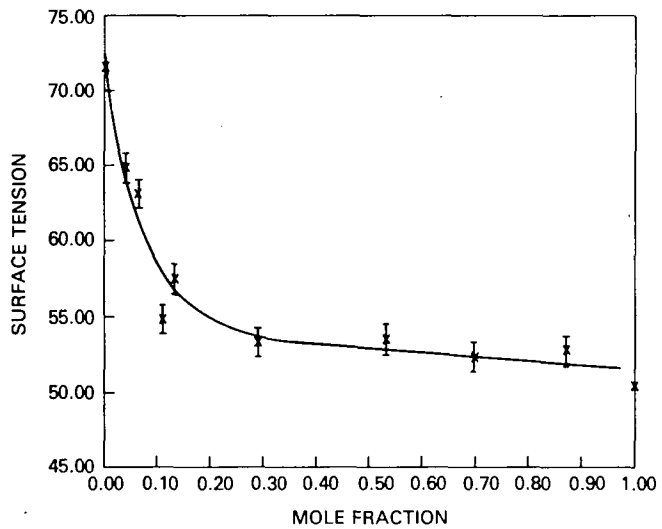

Fig. 11 — Curve fit to surface tension measurements provided by William Barger

The error bars in Fig. 11 indicate the repeatability of the measurement on a given solution but do not include any errors caused by mixing or impurities in the original MSA. The MSA was reagent grade obtained from Kodak.

The values of the equilibrium vapor pressure of MSA and water over solutions of MSA give the conditions necessary to saturate the atmosphere in the binary sense, i.e., any additional MSA or water vapor added to the saturated atmosphere would result in condensation of MSA solution on a wettable flat surface. Figure 12 shows the saturation curve. Conditions corresponding to points above the saturation curve are supersaturated with regard to MSA solutions. The numbers in parentheses (Fig. 12) gives the concentration in mole fraction of a solution that would be in equilibrium with the saturated atmosphere at the indicated RH.

4.2 Heterogeneous Nucleation

Heterogeneous nucleation refers to the nucleation of preexisting particles. When the supersaturation reaches a certain threshold, nuclei of a certain radius (and composition) will be nucleated. The higher the supersaturation the smaller will be the radius of the critical size nucleus. If the supersaturation is with respect to a binary solution, then the nucleation is referred to as binary heterogeneous nucleation. To circumvent the complications of dealing with nuclei of unknown composition that may be reactive with the condensate in one extreme, or in the other extreme, nonreactive and nonwettable, we assume that the particles are nonreactive but wettable (have zero contact angle) with the condensate. This assumption is equivalent to assuming the nuclei are of the same substance as the condensate. Under this assumption, the critical radius of the nuclei and composition of the condensate at the critical point are given by the saddle point of the free-energy surface. Figure 13 shows the free-energy surface as calculated from Eq. (5) using the thermodynamic data previously presented and for

UNCLASSIFIED

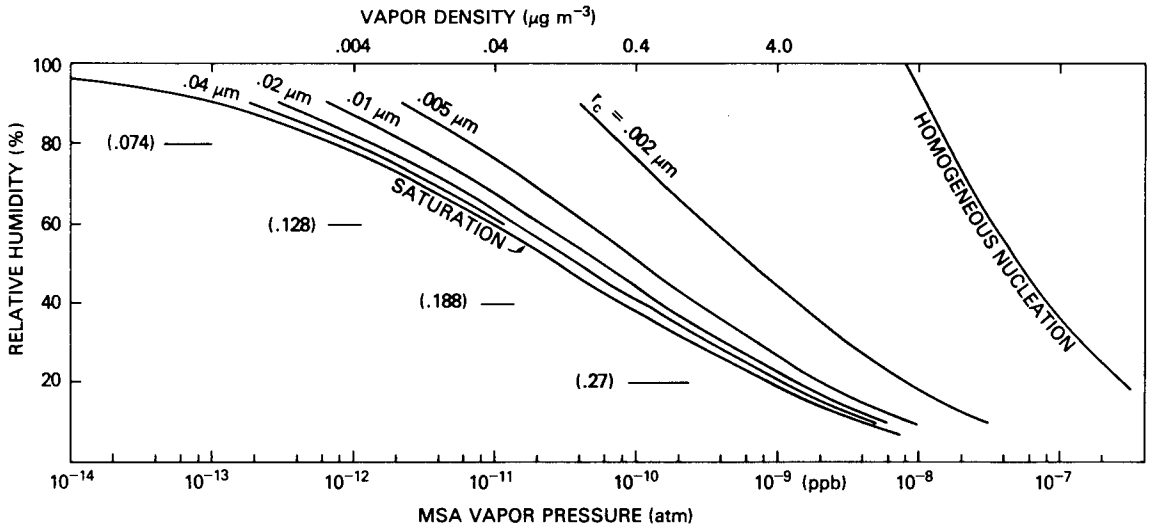

Fig. 12 — Curves showing the environmental conditions necessary to produce condensation of MSA solution on wettable walls (line labeled saturation) and heterogeneous and homogeneous nucleation curves give conditions necessary to cause condensation of MSA solution on wettable particles of the indicated radius. The homogeneous nucleation line gives the threshold conditions for spontaneous formation of new MSA solution embryos. The numbers to the left of the saturation line are the concentrations of MSA in a bulk MSA solution that is in equilibrium with a saturated environment at several values of environmental relative humidity.

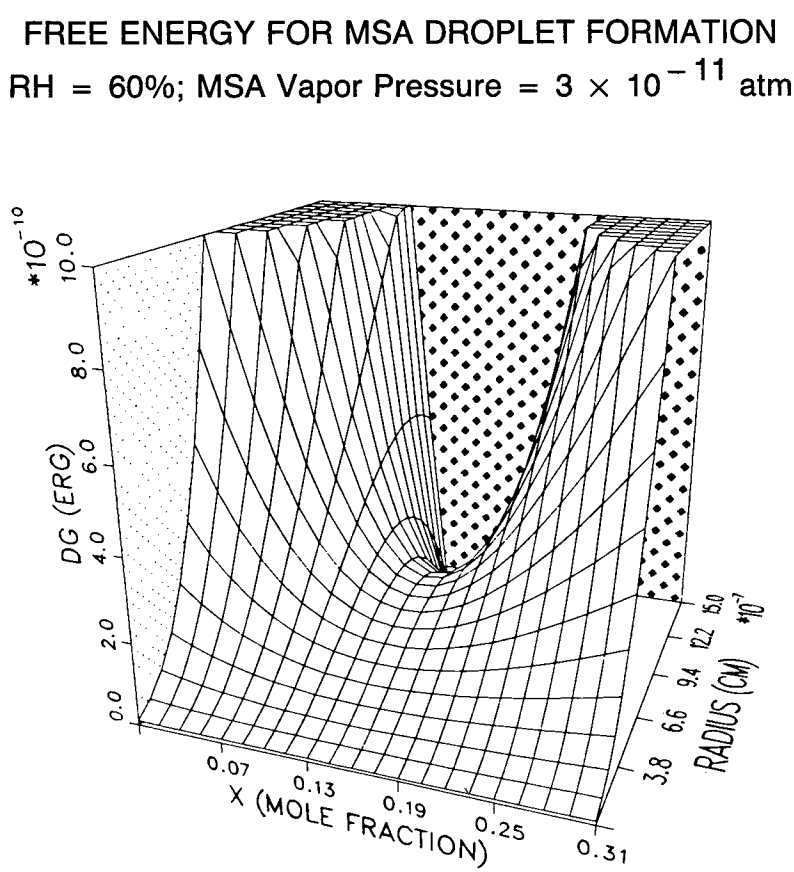

Fig. 13 — Free energy surface for 60% RH and an MSA vapor pressure of 3×10^{11} atm

environmental conditions of 60% relative humidity and 0.03 ppb MSA vapor pressure. The radius and MSA concentration at the saddle point are about 0.008 μm and 0.14 mole fraction respectively.

Figure 12 shows the conditions necessary to nucleate preexisting wettable particles of radius 0.04, 0.02, 0.01, 0.005, and 0.002 μm. These curves were obtained by finding the saddle point of the free-energy surface numerically for a large number of MSA and water vapor conditions. For a given relative humidity, it requires increasingly higher environmental concentrations of MSA to activate smaller particles.

4.3 Homogeneous Nucleation

Binary homogeneous nucleation occurs when the concentrations of MSA and water vapor are large enough for spontaneous formation of new particles directly from the vapor. Solution clusters are continuously being formed and destroyed. There is a finite probability that some of these embryos will grow large enough to become stable particles; i.e., the particle will exceed the critical radius and concentration and pass over the saddle point. The lower the energy barrier (saddle point), the higher is the probability of particle formation. At some point, as the environmental vapor pressures increase, the energy barrier will be low enough for a measurable number of embryos to grow into stable droplets. This point is the threshhold for homogeneous nucleation.

In contrast to the case of heterogeneous nucleation, which was treated as a static problem, homogeneous nucleation is a statistical process. Reiss (1950), Doyle (1961), Mirabel and Katz (1974), Stauffer (1976), and Binder and Stauffer (1976) have made substantial contributions to the theory of heteromolecular homogeneous nucleation theory. All of the theories give the following form for the nucleation rate

$$I = C \cdot \exp\left(-\frac{\Delta G_{sad}}{kT}\right), \tag{9}$$

where G_{sad} is the free energy at the saddle point, T is the temperature, and k is Boltzmann's constant. The differences in the theories are contained in the factor C. Calculating C is quite difficult and involves the kinetics of the process and evaluation of the directional derivatives of ΔG. In the calculations presented here, we have used the formulation of Stauffer (1976) as corrected and discussed by Mirabel and Clavelin (1978). Carrying out these calculations numerically results in the homogeneous nucleation line shown in Fig. 12.

The accuracy of the results shown in Fig. 12 depends on the accuracy of the thermodynamic data. The data with the largest uncertainty are the surface tension and the experimental data that relate the activity coefficient to the MSA vapor pressure. The surface tension does not affect the saturation curve and has only a small effect on heterogeneous nucleation of preexisiting particles larger than about 0.01 μm. Any errors in the surface tension will have considerable effect on the homogeneous nucleation threshold and heterogeneous nucleation of very small particles; whereas, any uncertainties in the equilibrium vapor pressure of MSA are probably the dominant source of error in the saturation curve and in the heterogeneous nucleation curves that lie close to the saturation curve. Our calculations are based on the best data currently available, and it is unlikely that future improvements in the accuracy of the data will significantly change the overall picture presented here.

4.4 Hydration of MSA Molecules in the Vapor Phase

Because of the strong binding energy between MSA and water, hydrate formation in the vapor phase is expected. The theory for hydration of H_2SO_4 in the presence of water vapor has been reported by Heist asnd Reiss (1974). This theory can also be applied to the hydration of MSA. For the calculations, both the water vapor and MSA vapor pressures must be specified. Pairs of these values that lie on the homogeneous nucleation curve were used in the calculations shown in Fig. 14,

UNCLASSIFIED

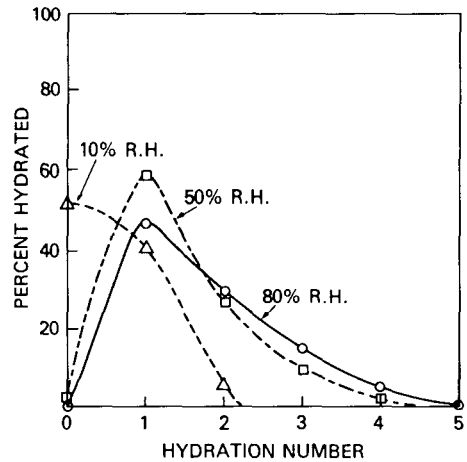

Fig. 14 — Fraction of MSA vapor molecules as a function of hydration number. Curves are drawn only to help distinguish the symbols

where the symbols indicate the fraction of MSA hydrated as a function of the number of water molecules in the hydrate for three values of relative humidity. The results shown were obtained by use of the method leading to Eq. (22) in Heist and Reiss (1974). At 50% RH, only a few percent of the MSA molecules are unhydrated, and about 60% of the hydrates contain only one water molecule.

Hydrate formation will, of course, affect the molecular properties such as the diffusion coefficient and thermal velocity; however, the mass of MSA is 96 amu, whereas the mass of the water molecule is only 18 amu. Therefore, hydration with a single water molecule is not expected to have a large effect on the kinetic properties of the molecule. Shugard and Reiss (1976) have shown that hydrate formation should be taken into consideration in homogeneous nucleation calculations and the effect of hydration is to decrease nucleation efficiency (increase the MSA concentration required for homogeneous nucleation). However the work of Mirabel and Clavelin (1978) with H_2SO_4 (where hydration is even more important) would indicate that, in our case, the effect of MSA hydration on the nucleation rate is small; certainly, smaller than errors resulting from uncertainties in the thermodynamic data.

4.5 Application to Results of Irradiation Experiments

From the measured rate of destruction of DMS and presumed conversion to MSA at the onset of irradiation, it is possible to estimate the maximum MSA vapor concentration by assuming no loss by condensation on particles. The time (after the start of irradiation) required for the MSA vapor to reach the threshold for homogeneous nucleation would be on the order of 1 h. Since new particle formation was observed in less than 5 min of irradiation, we conclude that the homogeneous nucleation was not that of pure MSA and water vapor. As pointed out earlier, Hatakeyama et al. (1985) estimated that in their experiments about 20% of the DMS converted to SO_2 with 80% conversion to MSA and that both H_2SO_4 and MSA were observed in their aerosol. Homogeneous nucleation of H_2SO_4 occurs at concentrations about three orders of magnitude lower than MSA. And it is known that other trace gases such as ammonia can also lower the nucleation threshold.

From the information currently available to us, we believe the nucleation of new particles in the chamber experiments was the result of heteromolecular homogeneous nucleation involving H_2SO_4 and possibly other trace gases. However, once the particles were nucleated and reached a radius of 0.005 μm or greater, then MSA and water vapor were the dominant condensing species that caused the growth observed over many hours that is discussed in the next chapter.

These results make it clear that additional experiments designed to look at the chemistry as well as the dynamics of the size distribution are necessary to understand the total gas-to-particle conversion process. It would also be helpful to develop the thermodynamics of the ternary system MSA-H_2SO_4 and water. Since the required thermodynamic data are not currently available, this would require laboratory measurements of the thermodynamics of the ternary solution.

5. MODELING THE TIME EVOLUTION OF PARTICLE-SIZE DISTRIBUTIONS WITH A DYNAMIC AEROSOL MODEL

Simulation of the dynamic behavior of an aerosol population is necessary to obtain an improved understanding of the dynamics of aerosol systems. Efforts to reconcile differences between modeled and observed aerosol behavior can lead to an improved theoretical description of the physical and chemical processes that govern aerosol evolution. The previous experiment in which aerosol formation and growth was observed when air containing DMS was irradiated with UV light, is an excellent case to simulate with a dynamic aerosol model. This experiment was conducted in a well-controlled environment and accurate measurements of the evolution of the particle-size distribution were obtained over a 7-h period. In addition, it was possible to estimate the generation rate of MSA, which was the driving force for the particle growth by condensation.

5.1 Description of Model

The equation governing aerosol dynamics, by which we mean the spatial and temporal variation of an aerosol population in response to various physical and chemical processes, is known as the general dynamic equation (GDE) for aerosols (Friedlander, 1977; Warren and Seinfeld, 1985). In recent years a number of mathematical models, based on the numerical solution of the GDE for a spatially homogeneous aerosol, has been developed to simulate aerosol dynamics. The model we selected for simulating aerosol dynamics in the Calspan chamber experiments is MAEROS-1A. This model is an improved version of the MAEROS model (Gelbard and Seinfeld, 1980; Gelbard, 1982) for multicomponent aerosol dynamics and incorporates a more accurate method for calculating condensational growth. The numerical technique used in MAEROS-1A for solving the GDE is based on dividing the particle size range into a discrete number of size classes or sections and imposing the condition of mass conservation for each chemical component. The model computes the evolution of the distributions of mass and number concentration with respect to particle size.

The physical processes included in MAEROS-1A are:

- particle coagulation due to Brownian motion, gravity, and turbulence;
- particle deposition due to settling, diffusion, thermophoresis, and diffusiophoresis;
- particle growth by condensation of a single vapor;
- time-varying sources of particles of different sizes and chemical compositions; and
- a time-dependent source of condensible vapor.

To properly simulate aerosol dynamics in the Calspan chamber experiment, it was necessary to modify the MAEROS-1A code to allow for binary condensation of both water vapor and MSA and for the loss of MSA vapor by diffusion to the inside surfaces of the chamber. A discussion of these two processes and the changes made to MAEROS-1A follows.

5.1.1 Condensation

The rate at which an aerosol particle grows by vapor condensation has a size dependence that is controlled by the Knudsen number, Kn, which is defined as the ratio of the mean free path of the condensable vapor to particle radius. In the free molecular regime ($Kn >> 1$), the condensation growth

UNCLASSIFIED

rate (dm/dt) is proportional to particle surface area, but in the continuum regime ($Kn << 1$), condensation is proportional to particle radius. The condensational growth law used in MAEROS-1A is the Fuchs-Sutugin formula (Fuchs and Sutugin, 1971), which is valid throughout the molecular, transition, and continuum regimes. The Fuchs-Sutugin equation may be written

$$\frac{dm}{dt} = 4\pi r D \left\{ \frac{1 + Kn}{1 + 1.71\,Kn + 1.33\,Kn^2} \right\} [\rho\,(\infty) - \rho(r)], \tag{10}$$

where m is particle mass, r is particle radius, D is the diffusivity of the condensing vapor in air, $\rho(\infty)$ is the ambient vapor density, and $\rho(r)$ is the vapor density at the surface of the particle. For a liquid particle composed of the pure condensate we have

$$\rho(r) = \rho^0 \exp \left[\frac{2\sigma}{r \rho_L R_v T} \right], \tag{10a}$$

where ρ^0 is the saturation vapor density over a plane surface of the condensed phase, ρ_L and σ are the density and surface tension of the pure condensed phase, R_v is the specific gas constant of the vapor, and T is temperature. The exponential term describes the Kelvin curvature effect.

Equation (10) describes droplet growth by condensation of a single vapor. The experiment we wish to simulate involves gas-to-particle conversion in a humid environment, and it is therefore necessary to modify the treatment of condensation growth in MAEROS-1A to take into account the binary condensation of both MSA vapor and water vapor. The theory of binary condensation is discussed by Hoppel (1975), and the analogous form of Eq. (10) for the binary condensation of water vapor and some gas phase species of low volatility (such as MSA) may be written

$$\frac{dm}{dt} = \frac{4\pi r D}{c} \left\{ \frac{1 + Kn}{1 + 1.71\,Kn + 1.33\,Kn^2} \right\} [\rho_s(\infty) - \rho_s(r,c)], \tag{11}$$

where m is the total mass of the particle (droplet) which is composed of an aqueous solution of water and the low volatility condensing species (referred to as the solute); c is the weight fraction of solute in the particle; $\rho_s(\infty)$ is the ambient vapor density of the solute; and $\rho_s(r,c)$, the vapor density of the solute at the surface of the particle, is a function of both r and c. The weight fraction of solute is related to the solute mole fraction, x, the more commonly used thermodynamic variable, through the expression

$$c = \frac{x M_s}{x M_s + M_w (1 - x)}, \tag{12}$$

where M_s and M_w are the molecular weights of the solute and water, respectively.

The calculation of particle growth by binary condensation requires that we know the values of c and $\rho_s(r,c)$ in addition to $\rho_s(\infty)$. Mirabel and Katz (1974) give the following expressions for the equilibrium vapor densities of the solute and water over the surface of an aqueous solution droplet of radius r:

$$\rho_s\,(r,x) = \rho_s^o(x) \exp \left\{ \frac{1}{R^*T} \left[\frac{2\sigma \bar{V}_s}{r} + \left[\frac{3(1-x)V}{r} \right] \frac{d\sigma}{dx} \right] \right\}, \tag{13}$$

and

$$\rho_w(r,x) = \rho_w^o(x) \exp \left\{ \frac{1}{R^*T} \left[\frac{2\sigma \bar{V}_w}{r} - \left[\frac{3xV}{r} \right] \frac{d\sigma}{dx} \right] \right\}, \tag{14}$$

where $\rho_s^o(x)$ and $\rho_w^o(x)$ are the equilibrium vapor densities of the solute and water over a plane (bulk) surface of a solution containing a mole fraction x of solute, $\bar{V}_s$ and $\bar{V}_w$ are the partial molar volumes, and V and $\sigma(x)$ are the molar volume and surface tension of the solution, respectively. To calculate $\rho_s(r,c)$ it is necessary to know the dependence of x (or c) on particle radius. Hoppel (1975) argues that since the rate of mass increase of the particle caused by water vapor condensation is just $(1 - c)/c$ times the mass increase caused by condensation of the solute (in spite of the fact that the water vapor density is many orders of magnitude greater than the vapor density of the low volatility solute), it follows that the difference between $\rho_w(r,x)$ and $\rho_w(\infty)$, the ambient water vapor density, must be exceedingly small. This means that x as a function of r can be determined from the condition $\rho_w(r,x) = \rho_w(\infty)$ provided we know ρ_w^o, σ, and droplet density as a function of x. Calculations of c as a function of droplet radius (Hoppel, 1975) show that c decreases as a droplet grows and approaches a constant value when the curvature effect becomes negligible (at a radius of about 10^{-5} cm). Once the concentration of solute is determined as a function of r, the particle growth rate can be calculated from Eq. (11).

To simplify the calculation of particle growth in the present model, the effect on particle curvature on the equilibrium vapor density was neglected and the values of x and $\rho_s(r,x)$ were assumed to be consant, independent of particle size, and equal to

$$x = x^o$$

$$\rho_s(r,x) = \rho_s^o(x^o) ,$$

where x^o and $\rho_s^o(x^o)$ are the solute mole fraction and solute vapor density of a bulk aqueous solution in equilibrium with the ambient RH.

Table 2 gives the equilibrium vapor pressures of MSA and water (the latter expressed as the water vapor saturation ratio) over a bulk MSA-water solution as a function of MSA mole fraction. Thus for example, to compute the growth of MSA-water solution droplets in an environment of 77% RH (saturation ratio equal to 0.77) we would use $x = 0.0825$ (or, from Eq. (12), $c = 0.324$) and $\rho_s(r,x) = 4.45 \times 10^{-12}$ kg/m^3, which corresponds to $p(r,x) = 1.15 \times 10^{-12}$ atm.

The neglect of the effect of particle curvature in calculating x and $\rho_s(r,x)$ will introduce little error in the calculated growth of a population of particles as long as $\rho_s(\infty)$ is sufficiently greater than $\rho_s(r,c)$ so that the curvature correction has only a small effect on the difference $\rho_s(\infty) - \rho_s(r,c)$.

5.1.2 Vapor Deposition on Walls

The loss of the low volatility condensable vapor by diffusion to the interior surfaces of the chamber is taken into account by adding to the equation for $d\rho_s(\infty)/dt$ the additional term

$$-\rho_s(\infty) v_d \frac{A}{V} ,$$

where v_d is the vapor deposition velocity, and A/V is the surface to volume ratio of the chamber. The time rate of change of $\rho_s(\infty)$ is thus determined by the competing effects of vapor generation, vapor consumption by the growing particles, and vapor loss to the walls. The vapor deposition velocity is defined as the flux of vapor to a surface divided by the vapor concentration at some reference distance from the surface.

5.2 Description of DMS Irradiation Experiments

The modified version of MAEROS-1A was used to simulate the evolution of particle-size distributions during the DMS irradiation experiment of 5-6 February 1986. This section gives a brief summary of the experiment and describes the observed evolution of the particle size distribution. A more complete discussion of the experiment is given in Section 3.2 of this report.

UNCLASSIFIED

The experiment began at 1715 on 5 Feb. 1986 when DMS was introduced into the chamber. The UV lights were turned on at 1735 and remained on for 8 h. A large concentration of small particles was detected with a Gardner counter 1 to 2 min after the lights were turned on. Particle production ceased after about 6 min, but the newly formed particles continued to grow. After 20 min, all particles had grown large enough to be within the range of the mobility analyzer. As discussed in Section 4 of this report, particle formation is believed to have resulted from heteromolecular homogeneous nucleation of H_2SO_4, water vapor, and possibly other trace gases. H_2SO_4 is formed by the photooxidation of SO_2. Both SO_2 and MSA are products of the photooxidation of DMS. Once the particles began to grow, the vapor concentrations were reduced below the level necessary for homogeneous nucleation and particle formation ceased. It is further speculated that growth of the particles beyond a radius of about 0.005 μm was due primarily to binary condensation of MSA and water vapor.

Figure 15 shows the observed evolution of the particle-size distributions over a 7-h period, as measured with the differential mobility analyzer. The distribution for $t = 0$ is the first measured distribution after all the particles had grown into the mobility analyzer size range. The other distributions were measured 0.35, 1.06, 2.53, 4.63, and 7.06 h after the initial distribution. The measurements show that there was a significant increase in particle size and a steady decrease in particle concentrations. The mode radius increased from 0.01 to 0.06 μm, while particle concentrations decreased from 123,000 to about 13,000 cm^{-3}. Because of the very low particle concentrations at the small end of the size distribution, the correction for multiply charged particles resulted in some negative values of dN/dr at the smaller sizes. The dashed portions of the size distributions are estimates of the distributions at the sizes where negative values of dN/dr occurred.

5.3 Simulation of Aerosol Evolution During DMS Irradiation Experiments

The measured size distribution for $t = 0$ in Fig. 15 served as the starting point for the numerical simulation of the evolution of the aerosol size distribution. The model was run with all of the aforementioned physical processes acting on the aerosol except for particle deposition due to diffusiophoresis and thermophoresis.

5.3.1 Inputs to Model

Principal inputs to the model and the values that were used in the present simulation (given in parentheses) include:

- the particle-size range (0.006 to 0.75 μm radius);
- the number of sections into which the size range is subdivided (20);
- the number of chemical components (one, MSA-water solution);
- the initial mass concentration in each section (calculated from the initial size distribution in Fig. 15);
- generation rate of MSA vapor (derived from the rate of decrease of gaseous sulfur in the chamber, the generation rate was found to decrease from 2.7×10^{-12} kg/(s m^3) at t = 0 to 1.07×10^{-12} kg/(s m^3) at t = 7.06 h;
- mass generation rate in each section due to new particle formation (zero);
- initial concentration of condensable vapor (3.5×10^{-11} kg/m^3, which is the smallest initial MSA concentration resulting in a monotonically decreasing MSA concentration with time);

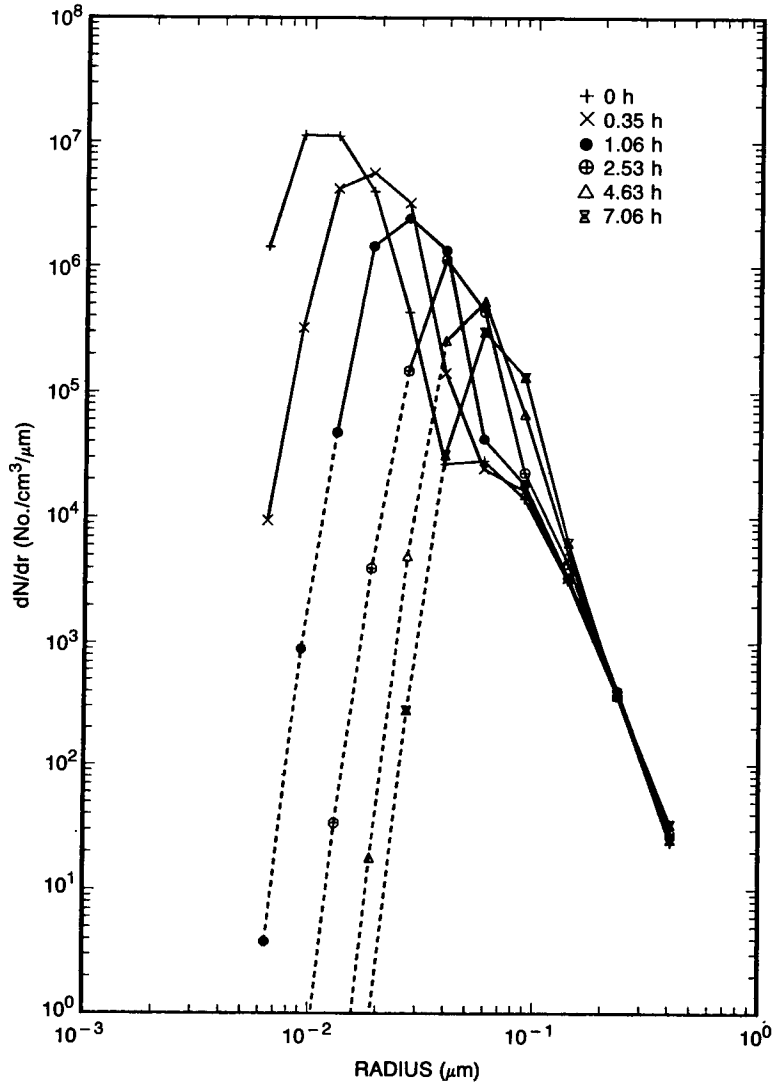

Fig. 15 — Observed evolution of the particle-size distribution during the DMS irradiation experiment of 5-6 February 1986

- the weight fraction of MSA in the particles, the equilibrium vapor density of MSA over the surface of the particles and the density of the particles (0.0825, 4.45×10^{-12} kg/m^3 and 1.15 g/cm^3, respectively, and equal to the values for a bulk MSA-water solution in equilibrium with the chamber relative humidity of 77%);

- the diffusivity of MSA vapor in air (0.1 cm^2/s);

- the ratio of the area of the ceiling, floor, and walls of the chamber to chamber volume (0.1094, 0.1094, and 0.4374, respectively); and

- temperature (298 K) and pressure (1010 mb).

Two additional input parameters, namely the diffusion boundary thickness at the inside surface of the chamber and the MSA vapor deposition velocity, exert a strong influence on the evolution of the particle-size distribution. Appropriate values of these parameters for conditions in the chamber cannot be estimated from measurements made during the experiment. Rather, it is necessary to base the selection of suitable values of these parameters on theoretical considerations and/or published data.

UNCLASSIFIED

The diffusion boundary layer thickness, δ, at the walls of the chamber has a significant effect on the decrease in particle concentrations with time since the diffusional deposition of particles, as formulated in the model, is proportional to the particle diffusion coefficient divided by δ. The concept of a diffusion boundary layer adjacent to the walls of a containment chamber strictly applies where natural convective motions within the chamber maintain a nearly uniform aerosol concentration, and particles diffuse to the walls through a quiescent boundary layer. The thickness of the boundary layer depends on a number of factors, including the nature of the wall surface (i.e., smooth vs rough) and particle radius (Harrison, 1978). (The present model assumed that δ is the same for all particle sizes.) In the case of a quiescent boundary layer adjacent to smooth walls Harrison (1979) reports values of δ in excess of 500 μm for latex particles smaller than 0.1 μm radius. Harrisons's results are in general agreement with those of Nolan (1941) and Gillespie and Langstroth (1951). The work of Stein et al. (1973), on the other hand, indicates values of δ one to two orders of magnitude smaller than those of Harrison. If a mechanical stirrer is used to maintain uniform aerosol concentrations (as was the case in Calspan's chamber), aerosol deposition can be enhanced due to impaction and turbulent flow and the effective boundary layer thickness could be smaller than in a quiescent chamber.

In view of the wide range in experimental values of δ even for static chamber conditions and of the additional complication in our case of forced mixing by a fan, the appropriate value of δ to use in the simulation is by no means obvious.

The MSA vapor deposition velocity controls the rate at which MSA diffuses to the walls and thus affects the concentration of MSA in the chamber and the growth rate of the particles. If the deposition velocity is small, then the loss of MSA vapor (to the walls) will be small compared to the MSA vapor generation rate as well as the rate of MSA consumption by the growing particles. In this case, MSA deposition on the walls will have little effect on the concentration of MSA in the chamber and on particle growth. On the other hand, if the deposition velocity is large, then the loss of MSA to the walls will significantly affect the particle growth rate.

The vapor deposition velocity, v_d, depends on a number of factors including atmospheric stability, the volatility of the gas, and the properties of the deposition surface. If water is present, then other factors influence the deposition velocity, such as the solubility of the vapor in water and chemical reactions occurring in the water phase. To our knowledge, there are no published measurements of the deposition velocity of MSA. Since MSA reacts in water and has a low vapor pressure over dilute MSA-water solutions, there will be a minimum back pressure or resistance to the transfer of MSA to a wet surface. Considering the moist conditions existing in the chamber during the experiments with DMS, the deposition velocity of MSA can be expected to be high. Recent measurements of the deposition velocity of nitric acid vapor in the free atmosphere (Huebert, 1983) indicate values in the range of 2 to 4 cm/s. Nitric acid, like MSA, reacts in water and has a low vapor pressure over dilute nitric acid-water solutions and it may not be unreasonable to speculate that the deposition velocity of MSA is of the same magnitude as that of nitric acid.

The customary way to carry out the simulation would be to run the model using best-estimate values of δ and v_d and then to compare the model-predicted and observed size distributions as a test of the model's predictive ability. However, in view of the large uncertainty in the appropriate values of δ and v_d for the conditions of the experiment and the sensitivity of the model-predicted aerosol evolution to the values of these parameters, it was felt that proceeding in this manner would not be a fair test of the model. Rather, we thought that a more reasonable approach to the simulation would be to select values of δ and v_d that would force agreement between the predicted and observed values of particle mode radius and particle number concentration at the end of the 7 h of aerosol evolution and then to determine if, for these same values of δ and v_d, the model successfully predicts the evolution of the particle-size distribution over the entire 7-h period.

5.3.2 Results of the Numerical Simulation

Figure 16 shows the model-predicted evolution of the aerosol size distribution. These results were obtained using $\delta = 17$ μm and $v_d = 12$ cm/s; these were the values of δ and v_d necessary to have the model predict the correct values of particle concentrations and mode radius at the end of 7 h. Figures 17 and 18 show the observed and predicted values of particle concentrations and mean particle radius as a function of time. The slight differences between the initial size distribution in Fig. 15 and that in Fig. 16 and between the initial measured and calculated particle concentrations in Fig. 17 are due to the different number of size classes used to describe the measured and calculated size distributions.

Although the values of δ and v_d were specifically chosen to force the model-predicted distribution to match the observed distribution at the end of 7 h, it is quite significant that the model accurately predicted the evolution of the size distribution over the entire 7-h period. This probably indicates that the model contains an adequate theoretical description of all the important physical and chemical processes affecting the aerosol and that, given the correct value of all input parameters, the model will accurately simulate aerosol dynamics.

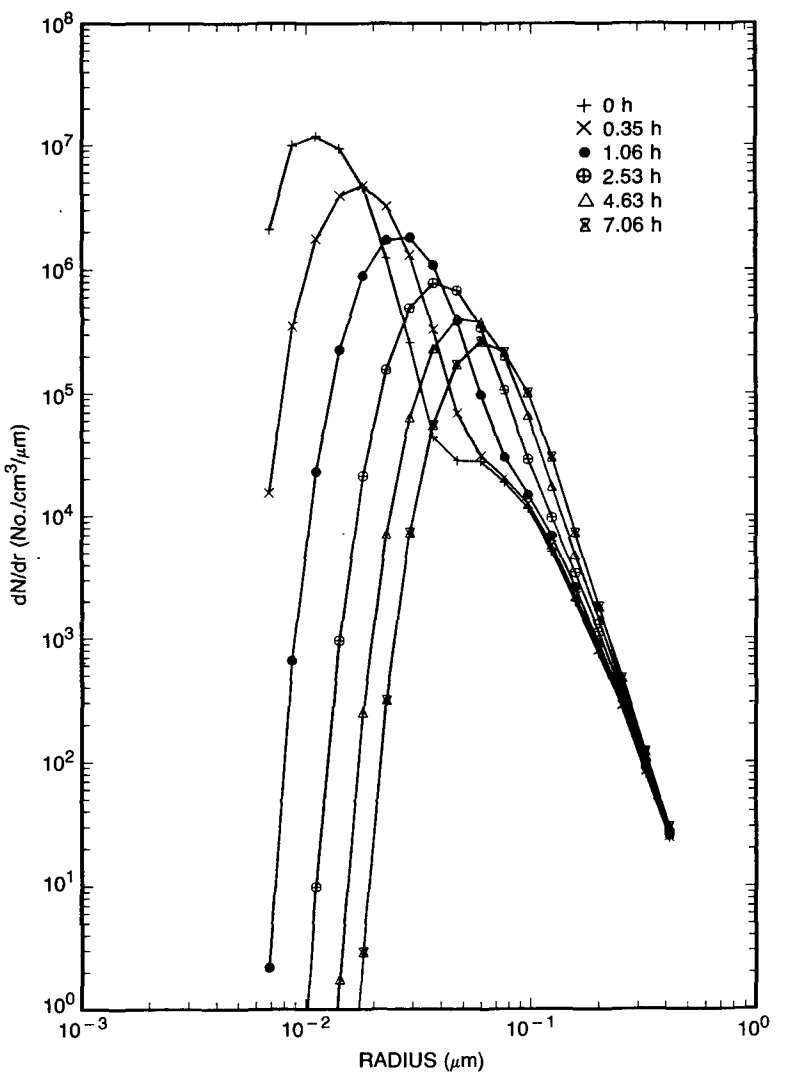

Fig. 16 — Model-predicted evolution of the particle size distribution during the DMS irradiation experiment of 5-6 February 1986

UNCLASSIFIED

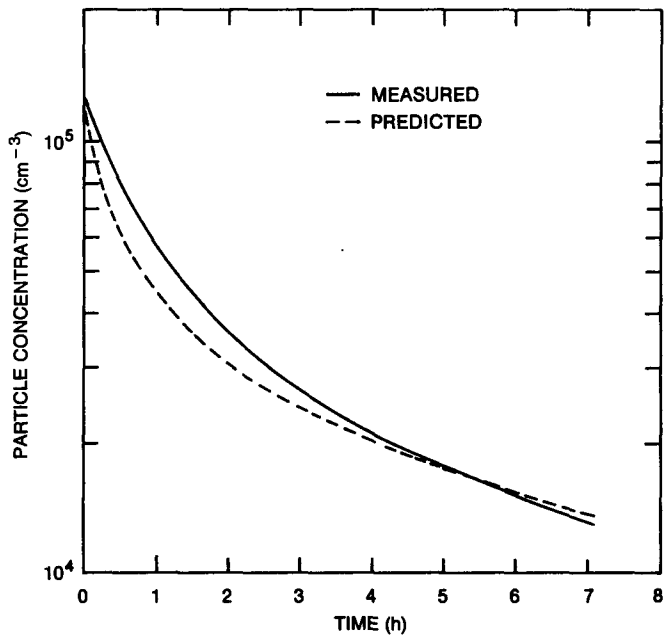

Fig. 17 — Comparison of observed and predicted evolution of particle concentration

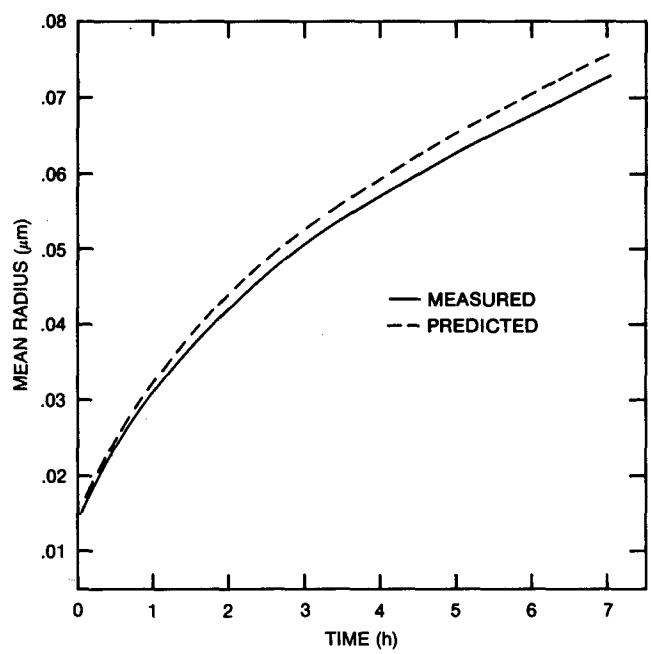

Fig. 18 — Comparison of observed and predicted evolution of mean particle radius

The only noteworthy differences between the predicted and observed distributions are that the predicted distributions are slightly broader after about 2 h and show a greater increase in the number of particles larger than 0.1 μm radius.

6. CONCLUSIONS

It is clear that the chamber experiments described in this report offer an excellent opportunity to isolate and study specific mechanisms that are believed to be important in the production and alteration of atmospheric aerosols. Comparisons of the observed evolution of the size distribution under well-defined conditions that exist in a chamber, with the evolution predicted by the dynamical aerosol model, make it possible to verify the model before applying it to the real atmosphere.

The results of these experiments demonstrate that DMS, the most abundant natural source of sulfur, is photooxidized to some product of low volatility (most likely MSA or H_2SO_4) that readily condenses on existing aerosol particles. Since one of the likely products of DMS photolysis is MSA, a study of the nucleation properties of MSA was undertaken. The nucleation thresholds calculated using thermodynamic data for MSA shows that at 70% RH an MSA concentration of only 0.006 ppb will result in a supersaturated environment in which MSA solution will condense on preexisting (wettable) particles larger than 0.02 μm radius (Fig. 12). If the concentration of MSA increases to about 30 ppb, then spontaneous formation of microscopic MSA solution droplets occurs by homogeneous binary nucleation.

Simulations of the evolution of the size distribution observed for the DMS irradiation experiments with a dynamic aerosol model that includes the effects of coagulation, growth by condensation, and particle and vapor deposition on the walls of the chamber yield results that are in excellent agreement with the observed evolution. The inputs to the model are: the initial measured size distribution, the rate of photolysis of DMS, the thermodynamic properties of MSA, the chamber geometry, and the deposition velocity.

One of the objectives of these experiments was to test the hypothesis that nonprecipitating cloud cycles play a major role in forming the aerosol size distribution and often are responsible for the doubly peaked size distributions observed over the oceans. The doubly peaked size distribution is presumed to be due to activation of the cloud nuclei portion of the aerosol, which as cloud droplets, absorb and convert trace gases to involatile material within the droplets. If a droplet then leaves the saturated environment of the cloud, its evaporation will produce particulate residue that is larger than the original nucleus.

We view our failure to observe a clear break in the size distribution as nondefinitive in regard to proving or disproving the hypothesis because the cloud could only be maintained for approximately 10 min in the chamber. A large loss of cloud droplets due to fallout occurred in all of the clouds formed. In the natural marine environment these droplets would evaporate back down to aerosol size in the dryer air beneath the cloud. The cloud cycling experiments should be repeated with trace gases that are known to promote aqueous phase conversion of absorbed gases so that the conversion will occur on a time scale observable in the chamber.

The experimental results described in this report must be considered as preliminary. It is clear that the products resulting from the photolysis of DMS are extremely effective in gas-to-particle formation. Our discovery of this phenomenon was fortuitous, and we were not prepared to examine it in isolation. The chamber contained unknown trace gases introduced by flushing the chamber with outside air. The chamber has the facility to remove trace gases by filtering the air through large charcoal filters; however, this capability had not been requested and therefore was not available at the time we used the chamber. These experiments should be repeated in a clean chamber where it can be determined which photochemically produced radicals are responsible for the chemical reactions.

UNCLASSIFIED

7. ACKNOWLEDGMENTS

We are indebted to William Barger of NRL's Chemistry Division for making the measurements of the surface tension of MSA solutions used in Fig. 11 of this report; also to Dr. Fred Gelbard for providing us a copy of the MAEROS-1A Fortran Code which served as a basis for the dynamical aerosol model used in the numerical calculations presented in Section 5. We also thank Dr. Paul Twitchell of ONR (Code 12) for his support of this work.

8. REFERENCES

Andreae, M.O. and H. Raemdonck (1983), "Dimethylsulfide in the Surface Ocean and the Marine Atmosphere: A Global View," *Science* **221**, 744-747.

Berthoud, A. (1929), "Quelques Propriétés Physico—Chimiques des Acides Êthane—et Methane sufonique," *Helv. Chim. Acta* **12**, 859-865.

Binder, K. and D. Stauffer (1976), "Statistical Theory of Nucleation, Condensation and Coagulation," *Adv. Phys.* **25**, 343-396.

Clegg, S.L. and P. Brimblecombe (1985), "The Solubility of Methanesulphonic Acid and Its Implications for Atmospheric Chemistry," *Environmental Technology Lett.* **6**, 269-278.

Covington, A.K., R.A. Robinson, and R. Thompson (1973), "Osmotic and Activity Coefficients for Aqueous Methane Sulfonic Acid Solutions at 25 deg C," *J. Chem. and Eng. Data* **18**, 422-423.

Cox, R.A. and F.J. Sandalls (1974), "The Photo-Oxidation of Hydrogen Sulphide and Dimethyl Sulphide in Air," *Atmospheric Environment* **8**, 1269-1281.

Doyle, G.J. (1961), "Self-Nucleation in the Sulfuric Acid-Water System," *J. Chem. Phys.* **35**, 795-799.

Fitzgerald, J.W., W.A. Hoppel, and M.A. Vietti (1982), "The Size and Scattering Coefficient of Urban Aerosol Particles at Washington, D.C., as a Function of Relative Humidity," *J. Atmos. Sci.* **39**, 1838-1852.

Friedlander, S.K. (1977), *Smoke, Dust and Haze*, Wiley-Interscience, New York.

Fuchs, N.A. and A.G. Sutugin (1971), "High Dispersed aerosols," in *Topics in Current Aerosol Research*, G.M. Hidy and J.R. Brock, editors, Pergamon Press, Oxford, Vol. 2, pp. 1-60.

Gelbard, F. (1982), "MAEROS User Manual," Sandia National Lab. Report SAND80-0822, Albuquerque, NM.

Gelbard, F. and J.H. Seinfeld (1980), "Simulation of Multicomponent Aerosol Dynamics," *J. Colloid Interface Sci.* **78**, 485-501.

Gillespie, T. and G.O. Langstroth (1951), "The Aging of Amonium Chloride Smokes," *Canad. J. Chem.* **29**, 201-216.

Harrison, A.W. (1979), "Quiescent Boundary Layer Thickness in Aerosol Enclosures Under Convective Stirring Conditions," *J. Colloid Interface Sci.* **69**, 563-570.

Hatakeyama, S., K. Izumi, and H. Akimoto (1985), "Yield of SO_2 and Formation of Aerosol in the Photo-Oxidation of DMS Under Atmospheric Conditions," *Atmospheric Environment* **19**, 135-141.

Hanley, J.T., B.J. Wattle, and E.J. Mack (1981), "Extinction Characteristics of Pyrotechnical-Generated Alkali-Halide Smokes," Calspan Report 6855-M-1, Calspan Corporation.

Hoppel, W.A. (1975), "Growth of Condensation Nuclei by Heteromolecular Condensation," *J. Rech. Atmos.* **9**, 167-180.

Hoppel, W.A. (1978), "Determination of the Aerosol Size Distribution from the Mobility Distribution of the Charged Fraction of Aerosols," *J. Aerosol Sci.* **9**, 41-54.

Hoppel, W.A. (1981), "Measurement of the Aerosol Size Distribution with NRL's Mobility Analyzer," *J. Rech. Atmos.* **15**, 313-319.

Hoppel, W.A., J.W. Fitzgerald, and R.E. Larson (1983), "Measurement of Atmospheric Aerosols: Experimental Methods and Results of Measurements off the East Coast of the United States," NRL Report 8703.

Hoppel, W.A., J.W. Fitzgerald, and R.E. Larson (1985), "Aerosol Size Distributions in Air Masses Advecting off the East Coast of the United States," *J. Geophys. Res.* **90**, 2365-2379.

Hoppel, W.A., G.M. Frick, and R.E. Larson (1986), "Effect of Nonprecipitating Clouds on the Aerosol Size Distribution in the Marine Boundary Layer," *Geophys. Res. Lett.* **13**, 125-128.

Heist, R.H. and H. Reiss (1974), "Hydrates in Supersaturated Binary Sulfuric Acid-Water Vapor," *J. Chem. Phys.* **61**, 573-581.

Huebert, B.J. (1983), "Measurements of the Dry-Deposition Flux of Nitric Acid Vapor to Grasslands and Forests," in *Precipitation Scavenging, Dry Deposition, and Resuspension,* Elsevier, New York, pp. 785-792.

Mack, E.J., R.J. Anderson, and J.T. Hanley (1978), "A Preliminary Investigation of the Production of Stable Fogs Under Subsaturated Conditions," Calspan Report 6287-M-1, Calspan Corp.

McMurray, P.H. and S.K. Friedlander (1986), "Aerosol Formation in Reacting Gases: Relation to Surface Area to Rate of Gas-to-Particle conversion," *J. Colloid. Interface Sci.* **64**, 248-257.

Mirabel, P. and J.L. Clavelin (1978), "On the Limiting Behavior of Binary Homogeneous Nucleation Theory," *J. Aerosol Sci.* **9**, 219-225.

Mirabel, P. and J.L. Katz (1974), "Binary Homogeneous Nucleation as a Mechanism for the Formation of Aerosols," *J. Chem. Phys.* **60**, 1138-1144.

Nolan, P.J. (1941), "Experiments on Condensation Nuclei," *Proc. Roy. Irish Acad.* **47A**, 25-38.

Pich, J., S.K. Friedlander, and F.S. Lai (1970), "Size Distributions of Pollution Aerosols," *J. Aerosol Sci.* **1**, 115-120.

Pruppacher, H.R. and J.D. Klett (1978), *Microphysics of Clouds and Precipitation*, D. Reidel, Hingham, Mass.

Reiss, H. (1950), "The Kinetics of Phase Transitions in Binary Systems," *J. Chem. Phys.* **18**, 840-848.

Saltzman, E.S., D.L. Savoie, R.G. Zika, and J.M. Prospero (1983), "Methane Sulfonic Acid in the Marine Atmosphere," *J. Geophys. Res.* **88**, 10,897-10,902.

UNCLASSIFIED

Shugard, W.J. and H. Reiss (1976), "Transient Nucleation in H_2O-H_2SO_4 Mixtures: A Stochastic Approach," *J. Chem. Phys.* **65**, 2728-2840.

Stein, R.L., W.H. Ryback, and A.W. Sparks (1973), "Deposition of Aerosols in a Plastic Chamber," *J. Colloid Interface Sci.* **42**, 441-447.

Stauffer, D. (1976), "Kinetic Theory of Two-Component ("Heteromolecular") Nucleation and Condensation," *J. Aerosol Sci.* **7**, 319-333.

Sze, N.D. and M.K.W. Ko (1980), "Photochemistry of COS, CS_2, CH_3SCH_3, and H_2S: Implications for the Atmospheric Sulfur Cycle," *Atmospheric Environment* **14**, 1223-1239.

Teng, T.T. and F. Lenzi (1975), "Methanesulfonic and Trichloroacetic Acids: Densities of Aqueous Solutions at 20°, 25° and 35°C," *J. Chem. Eng. Data* **20**, 432-434.

Warren, D.R. and J.H. Sienfeld (1985), "Simulation of Aerosol Size Distribution Evolution in Systems with Simultaneous Nucleation, Condensation and Coagulation," *Aerosol Sci. Technol.* **4**, 31-43.